Available online at www.sciencedirect.com
ScienceDirect
Lithos 102 (2008) 218–236
LITHOS
www.elsevier.com/locate/lithos

Geochronology and geochemistry of Permian basalts in western Guangxi Province, Southwest China: Evidence for plume-lithosphere interaction

Weiming Fan *, Chunhong Zhang, Yuejun Wang, Feng Guo, Touping Peng

Key Laboratory of Isotope Geochronology and Geochemistry, Guangzhou Institute of Geochemistry, Chinese Academy of Sciences, Guangzhou 510640, China

Received 25 October 2006; accepted 24 September 2007
Available online 11 October 2007

Abstract

The Emeishan flood basalts are part of an important large igneous province (LIP) along the western margin of the Yangtze Block, Southwest China. Mafic rocks interlayered with Permian sedimentary rocks in western Guangxi Province, on the southeastern margin of the Yangtze Block, have SHRIMP zircon U–Pb weighted mean ages of 259.6±5.9 Ma and 259.1±4.0 Ma, identical to mafic plutons associated with the Emeishan basalts. The basaltic rocks, which are SiO_2-poor, and FeO-, TiO_2- and P_2O_5-rich, geochemically resemble the Emeishan high-Ti basalts. These rocks are enriched in large ion lithophile elements (LILE) and light rare earth elements (LREE), and have (Nb/La)n=0.75–0.94 and (Hf/Sm)n=0.78–0.90. They are characterized by moderate $^{86}Sr/^{87}Sr(i)$ ratios (0.704922–0.705804), intermediate $\varepsilon_{Nd}(t)$ values (−0.23 to 1.50), high $^{206}Pb/^{204}Pb_I$ ratios (18.77–19.67) and prominent positive Δ8/4 (67.7–82.7) and Δ7/4 (0.96–8.19) values. These geochemical signatures are also comparable to the Emeishan high-Ti basalts and the associated high-Ti intrusions in SW China, and might be attributed to low degrees of melting of a garnet-bearing mantle source. The elemental and isotopic compositions suggest that the magma source reservoir may have involved HIMU- and EM1-components, indicative of plume-lithosphere interaction at the periphery of the plume. We propose that these basalts in western Guangxi Province are spatially and temporally associated with the Emeishan LIP and that the Emeishan flood basalts extend over a broader region than previously thought.

Keywords: Basalt; SHRIMP zircon geochronology; Permian; Plume–lithosphere interaction; Emeishan large igneous province; Guangxi Province

1. Introduction

The Emeishan flood basalt is part of an important LIP covering an area of more than 500,000 km^2 along the western margin of the Yangtze Block, Southwest China (Fig. 1a). The LIP was formed at the Permian and Triassic boundary at about 260 Ma (Yin et al., 1992; Chung and Jahn, 1995; Song et al., 2001; Xu et al., 2001, 2004; Lo et al., 2002; Zhou et al., 2002a,b, 2006; Ali et al., 2004; Guo et al., 2004; Xiao et al., 2004a,b). He et al. (2003, 2006) divided the LIP spatially into 3 zones (Inner, Intermediate and Outer) on the basis of the bio-stratigraphic, sedimentological and geochemical characteristics. Previous studies suggested that the Emeishan

* Corresponding author. Current address: Guangzhou Institute of Geochemistry, Chinese Academy of Sciences, P.O. Box 1131, Guangzhou 510640, PR China. Tel.: +86 20 85290227; fax: +86 20 85291510.
E-mail address: wmfan@gig.ac.cn (W. Fan).

0024-4937/$ - see front matter © 2007 Elsevier B.V. All rights reserved.
doi:10.1016/j.lithos.2007.09.019

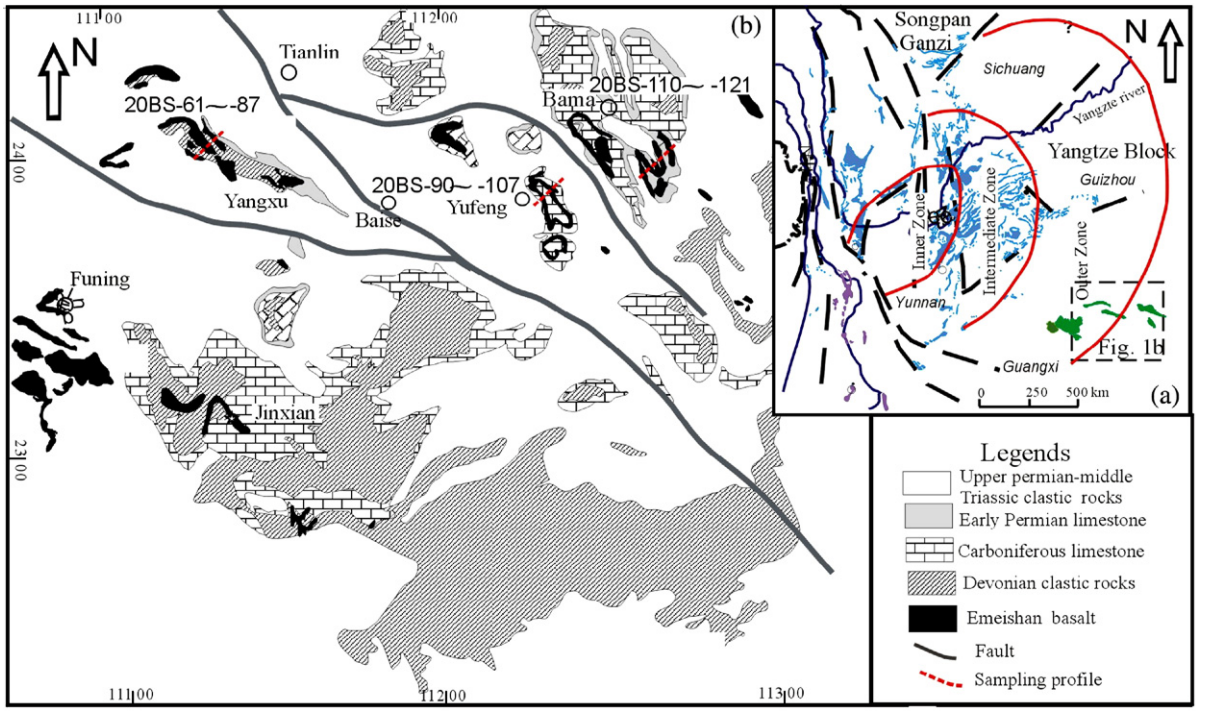

Fig. 1. (a) Schematic map showing the Inner, Intermediate and Outer zones of the Emeishan LIP (after Xu et al., 2001; He et al., 2003); (b) Geological map of western Guangxi Province showing the location of the Permian basalts described in this paper (after GXBGMR, 1985).

magmatism occurred mostly in the Inner and Intermediate zones, as indicated by exposures in Sichuan, Yunnan and Guizhou Provinces, and that only a few basalts are present in the Outer zone. The magmatic rocks of the Emeishan LIP are represented by voluminous outcrops of high-Ti and low-Ti basalts, mafic–ultramafic layered intrusions and associated alkaline and felsic rocks (Song et al., 2001; Xu et al., 2001, 2004; Xiao et al., 2004a,b; Zhou et al., 2002a,b, 2006; Ma et al., 2003). This rock association is similar to that in many other LIPs, such as the Siberian Traps, and is considered to reflect derivation from mantle plumes that underwent complex magmatic processes (Lightfoot et al., 1994; Arndt et al., 1998, 2003). Recent geochemical studies have shown that the high- and low-Ti rocks of the Emeishan LIP may have originated from distinct mantle sources under variable melting conditions (Chung and Jahn, 1995; Xu et al., 2001, 2004; Xiao et al., 2004a,b). The low-Ti basalts have a significant contribution from the subcontinental lithosphere mantle but the origin of the high-Ti magmas is not clear. Xu et al. (2001) suggested that these mafic magmas might have undergone an assimilation–fractionation–crystallization (AFC) style of evolution in the upper crust or to have resulted from interaction with gabbro-derived melts near the crust–mantle boundary. In contrast, Xiao et al. (2003, 2004a,b) concluded that the high-Ti magma was derived from a deep mantle plume.

Numerous bodies of layered mafic–ultramafic rocks crop out in western Guangxi Province, a region spatially corresponding to the Outer zone of the Emeishan LIP (Fig. 1a). These high TiO_2 rocks have traditionally been depicted as Hercynian diabase (e.g., GXBGMR, 1985), interlayered with deep-water sedimentary rocks, suggesting formation in an intra-oceanic setting (Wu et al., 1993; Wang et al., 1997). Based on recently obtained whole-rock $^{40}Ar/^{39}Ar$ plateau ages of 254–256 Ma for three basalts from the Baise area (western Guangxi) Fan et al. (2004) proposed that these rocks represent a distal part of the Emeishan LIP. However, the reported $^{40}Ar/^{39}Ar$ plateau ages are somewhat younger than the SHRIMP zircon U–Pb ages (258–261 Ma) of Emeishan LIP-related mafic–ultramafic intrusive rocks (e.g., Zhou et al., 2002a,b, 2006; Guo et al., 2004), indicating that more detailed geochronological data were needed to verify the proposed relationship of these basalts with the Emeishan LIP. Several other issues, such as whether the mantle source of the Guangxi high-Ti rocks is consistent with that of the Emeishan high-Ti flood basalts, also needed to be addressed properly.

In this paper, we present a set of new SHRIMP zircon U–Pb ages and whole-rock geochemical and isotopic

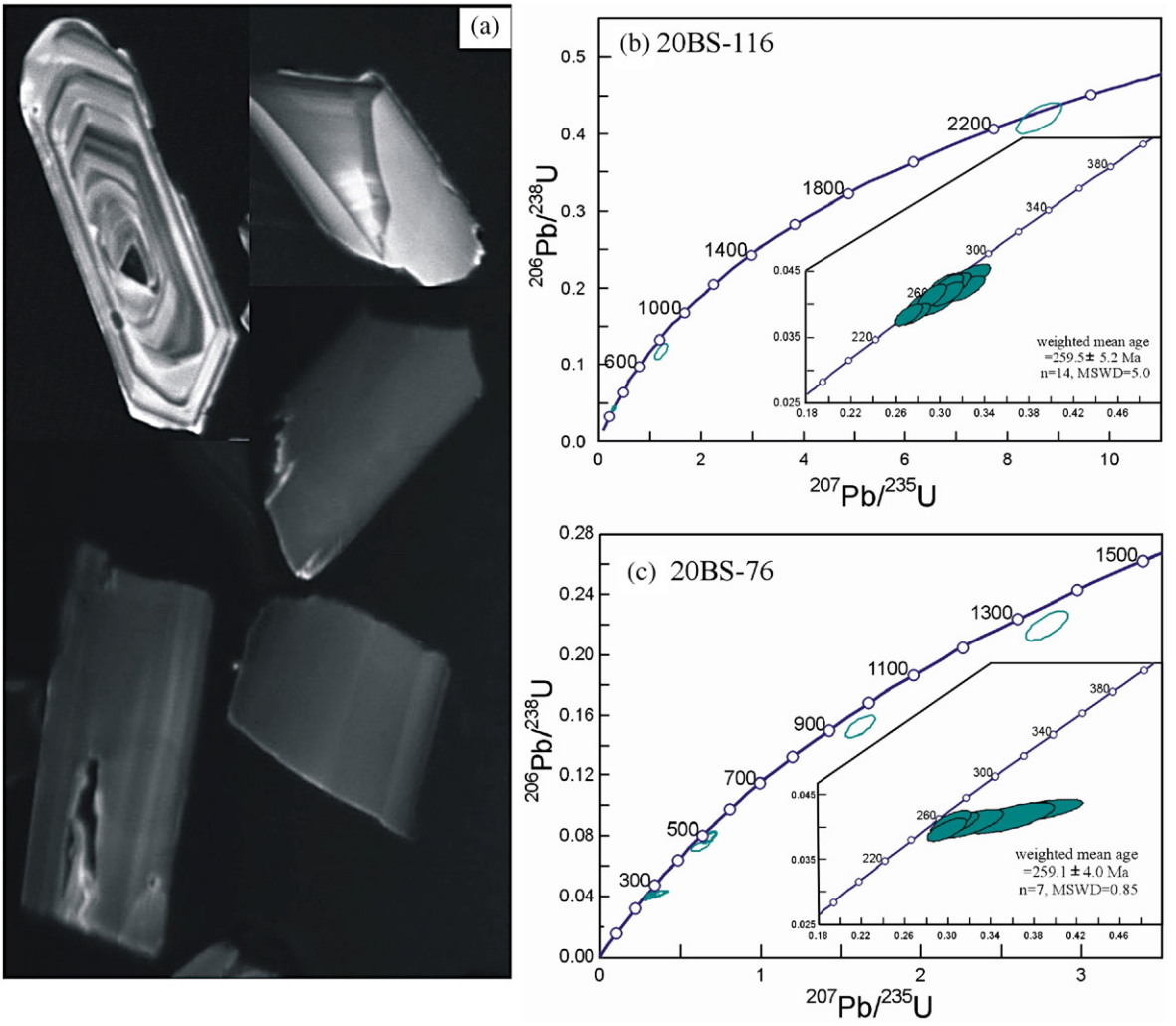

Fig. 2. (a) Cathodoluminescence images of representative zircons. (b) SHRIMP zircon U–Pb concordia plots for basalt sample 20BS-116 (Min'an area, Bama County), and (c) Sample 20BS-76 (Yangxu area, Baise County), western Guangxi Province (see Fig. 1b for locations of the samples).

data for basalts from three typical sections in western Guangxi Province. Using these data we attempt; (1) to shed light on the nature of the mantle source and on the role of plume-lithosphere interaction in the origin of the high Ti-basalts; and (2) to better constrain the regional distribution and ages of the Emeishan LIP.

2. Geological setting, field relationships and petrography

Western Guangxi Province in southwestern China is geologically a part of the Yangtze Block, which is characterized by having a Precambrian basement with Paleoproterozoic and Archean crystallization ages (Qiu et al., 2000). As shown in Fig. 1a, this area is located roughly in the Outer zone of the Emeishan LIP proposed by He et al. (2003, 2006). The exposed stratigraphic sequence in this area consists mainly of upper Devonian clastic rocks, Carboniferous and lower Permian limestone and upper Permian–middle Triassic clastic rocks (Fig. 1b). The magmatic rocks are predominantly late Paleozoic mafic volcanic rocks.

The volcanic rocks crop out chiefly in the Xilin–Longlin, Yangxu–Badu, Bama–Yixu, Yufeng and Napo areas in western Guangxi Province (Fig. 1b), in the Funing area of eastern Yunnan Province and the Weiyuan area in southern Guizhou Province (YNBGMR, 1990; GZBGMR, 1987; Zhou et al., 2006). Within these areas, the thickness of he volcanic sequence ranges from 300 m to 500 m. Previous studies (YNBGMR, 1990;

Table 1
SHRIMP zircon U–Pb dating results of 20BS-116 basalts (Bama) in western Guangxi Province, SW China

Analytical spot		Concentration (ppm)				Calculated ratio			Calculated apparent age (Ma)		
		U	Th	Pb*	Th/U	$^{206}Pb/^{238}U$	$^{207}Pb/^{235}U$	$^{207}Pb/^{206}Pb$	$^{206}Pb/^{238}U$	$^{207}Pb/^{235}U$	$^{207}Pb/^{206}U$
A1.1	20BS-116; Min'an, Bama	4793	26118	433	5.4490	0.04119±0.00150	0.29270±0.0108	0.05150±0.00040	260.2±9.0	260.7±8.5	264.7±17.2
A2.1		4381	10106	282	2.3069	0.04292±0.00150	0.31180±0.0126	0.05270±0.00080	270.9±9.4	275.6±9.8	315.4±36.3
A3.1		3723	18521	344	4.9751	0.04289±0.00154	0.31299±0.01203	0.05292±0.00054	270.7±9.5	276.5±9.4	325.5±23.2
A4.1		3553	17389	320	4.8945	0.04271±0.00153	0.30371±0.01220	0.05158±0.00074	269.6±9.4	269.3±9.6	266.7±33.5
A5.1		2811	10324	215	3.6734	0.04157±0.00147	0.30700±0.01187	0.05356±0.00063	262.6±9.1	271.9±9.3	352.7±26.7
A6.1		4347	21728	377	4.9985	0.04106±0.00149	0.29150±0.01119	0.05149±0.00045	259.4±9.2	259.7±8.8	263.0±20.4
A7.1		3978	19315	356	4.8562	0.04264±0.00150	0.30683±0.01183	0.05218±0.00061	269.2±9.3	271.7±9.2	293.5±27.0
A8.1		5631	27851	468	4.9462	0.04024±0.00143	0.28385±0.01105	0.05116±0.00061	254.3±8.9	253.7±8.8	247.9±27.8
A9.1		5957	25666	442	4.3086	0.03833±0.00139	0.27160±0.01025	0.05140±0.00037	242.5±8.6	244.0±8.2	258.7±16.7
A10.1		2202	2598	118	1.1800	0.04402±0.00169	0.32614±0.01592	0.05373±0.00138	267.7±8.5	286.6±12.3	359.8±58.9
A11.1		2200	5945	141	2.7023	0.04003±0.00142	0.29754±0.01264	0.05391±0.00104	253.0±8.8	264.5±9.9	367.5±44.3
A12.1		1756	4991	122	2.8418	0.04240±0.00157	0.32279±0.01463	0.05522±0.00121	267.7±9.7	284.1±11.3	421.1±49.8
A13.1		126	145	19	1.1497	0.11757±0.00871	1.22920±0.10532	0.07583±0.00263	716.6±50.5	814.0±49.1	1090.6±71.1
A14.1		152	103	74	0.6756	0.42060±0.01637	8.61420±0.36335	0.14854±0.00180	2263.2±74.7	2298.1±39.1	2329.2±20.9
A15.1		3769	22281	335	5.9122	0.03853±0.00137	0.27827±0.01063	0.05239±0.00054	243.7±8.5	249.3±8.5	302.3±23.8
A16.1		791	1399	43	1.7696	0.03909±0.00171	0.34604±0.03383	0.06420±0.00527	247.2±10.6	301.7±25.8	748.4±184

Table 2
SHRIMP zircon U–Pb dating results of the 20BS-76 basalts (Yangyu) in western Guangxi Province, SW China

Analytical spot		Concentration (ppm)				Calculated ratio			Calculated apparent age (Ma)		
		U	Th	Pb*	Th/U	$^{206}Pb/^{238}U$	$^{207}Pb/^{235}U$	$^{207}Pb/^{206}Pb$	$^{206}Pb/^{238}U$	$^{207}Pb/^{235}U$	$^{207}Pb/^{206}U$
E1.1	20BS-76; Yangyu, Baise	147	78	24	0.5343	0.15225±0.00588	1.62270±0.07376	0.07730±0.00151	913.5±33.0	979.1±28.9	1129±40
E2.1		261	123	20	0.4725	0.07339±0.00275	0.62480±0.04544	0.06175±0.00357	456.5±16.5	492.8±28.8	665±129
E3.1		1846	3687	107	1.9971	0.03953±0.00145	0.29949±0.01513	0.05495±0.00167	259.9±9.0	266.0±11.9	410±69
E4.1		2093	3411	115	1.6294	0.04041±0.00145	0.30808±0.01709	0.05529±0.00211	255.4±9.0	272.7±13.4	424±87
E5.1		2347	4719	137	2.0111	0.04056±0.00153	0.30278±0.01537	0.05414±0.00160	256.3±9.5	268.6±12.1	377±68
E6.1		519	178	22	0.3434	0.04229±0.00248	0.35453±0.03290	0.06081±0.00395	267.0±15.4	308.1±24.9	632±147
E7.1		812	1825	177	0.2244	0.21894±0.00810	2.78200±0.10669	0.09216±0.00060	1276.3±43.0	1350.7±29.1	1471±13
E81		3577	9334	205	2.6096	0.03520±0.00125	0.26482±0.01371	0.05457±0.00182	223.0±7.8	238.5±11.1	394.7±76.6
E9.1		4924	24368	388	4.9485	0.03704±0.00133	0.27555±0.01292	0.05396±0.00140	234.5±8.3	247.1±10.3	369.3±59.5
E10.1		505	851	29	1.6846	0.04134±0.00194	0.35821±0.03387	0.06285±0.00481	261.1±12.0	310.9±25.6	703±171
E11.1		2228	4370	137	1.9614	0.04046±0.00176	0.32104±0.02495	0.05755±0.00341	255.7±11.0	282.7±19.4	512±135
E12.1		511	966	32	1.8915	0.04229±0.00157	0.38047±0.03733	0.06524±0.00563	267.0±9.7	327.4±27.8	782±192
E13.1		455	98	36	0.0024	0.07936±0.00810	0.68012±0.03357	0.06215±0.00154	492.3±18.8	526.8±20.5	679±54
E14.1		3814	16760	278	4.3948	0.03555±0.00128	0.25570±0.01154	0.05217±0.00120	225.2±8.0	231.2±9.4	292.9±53.2

Table 3
Major and trace element abundances of Permian basalts from western Guangxi Province, SW China

Sample	20BS-61	20BS-63	20BS-65	20BS-66	20BS-69	20BS-71	20BS-73	20BS-75	20BS-78	20BS-80	20BS-81	20BS-84	20BS-85	20BS-87
Yangyu–Pingxu area, Baise County														
SiO_2	45.48	45.35	46.02	45.51	45.36	45.86	49.04	48.24	45.73	45.56	45.71	47.84	48.31	48.35
TiO_2	2.90	2.93	2.97	3.06	2.90	3.30	2.60	3.15	3.06	3.08	3.08	3.08	2.80	2.86
Al_2O_3	14.17	14.04	13.78	13.98	13.88	13.95	14.34	14.39	13.83	13.88	13.86	13.51	13.62	13.20
MgO	6.24	6.03	5.90	5.93	5.95	5.90	5.06	5.30	5.90	5.94	6.03	5.51	5.60	5.69
Fe_2O_3	2.20	1.78	2.40	2.16	2.83	1.62	2.67	2.03	2.17	2.04	2.05	1.98	1.82	2.03
FeO	11.17	11.60	10.63	11.67	10.50	12.03	9.73	9.37	11.63	11.60	11.80	11.07	10.57	11.07
CaO	9.11	10.24	10.29	9.56	10.47	9.81	8.95	9.63	9.70	9.72	9.97	9.65	9.79	9.28
K_2O	1.47	1.42	0.84	1.56	1.09	1.43	1.43	1.24	1.17	1.07	0.99	0.97	0.74	0.98
Na_2O	2.49	2.26	3.03	2.43	2.63	2.18	2.40	2.10	2.39	2.70	2.59	2.51	3.13	2.74
P_2O_5	0.52	0.54	0.53	0.56	0.52	0.56	0.48	0.46	0.56	0.56	0.55	0.54	0.44	0.44
MnO	0.21	0.21	0.20	0.21	0.21	0.22	0.19	0.21	0.23	0.22	0.22	0.23	0.23	0.22
LOI	3.20	3.31	3.15	3.07	3.36	3.12	2.85	3.63	3.32	3.33	2.89	2.97	2.70	2.83
Total	99.66	99.71	99.74	99.70	99.70	99.98	99.74	99.75	99.69	99.70	99.74	99.76	99.75	99.69
mg#	0.46	0.45	0.45	0.44	0.45	0.44	0.43	0.46	0.44	0.44	0.44	0.44	0.45	0.44
Cr	112.6	73.1	74.7	74.0	72.2	68.9	65.8	86.7	74.1	75.9	74.7	105.8	120.9	110.6
Ni	71.3	75.6	69.9	72.9	69.3	69.4	67.5	60.3	71.4	72.4	70.7	63.0	72.7	75.2
Rb	25.7	34.1	22.4	21.3	33.4	31.1	34.6	33.5	29.3	24.7	22.0	29.4	24.2	27.5
Sr	481	505	541	576	514	461	390	393	532	571	574	354	383	482
Y	24.90	27.51	25.16	26.46	26.89	26.68	36.56	35.62	30.76	27.14	27.60	33.79	34.00	32.90
Zr	138	142	139	148	152	149	211	196	148	150	148	189	189	178
Nb	22.21	23.36	23.11	23.74	25.09	24.47	27.87	29.04	24.04	25.24	24.30	26.78	28.32	24.75
Cs	1.61	4.00	4.84	2.71	2.00	2.00	3.07	5.00	4.35	3.34	3.16	1.86	1.52	1.81
Ba	1092	736	603	1052	974	762	452	460	1041	571	583	365	340	638
La	27.24	28.75	28.75	29.57	30.23	30.04	31.78	29.86	30.87	30.34	29.55	28.05	29.32	27.50
Ce	61.72	65.42	64.99	66.48	67.81	67.29	70.93	66.21	67.80	68.65	66.14	63.31	65.83	61.91
Pr	7.66	8.23	8.10	8.24	8.47	8.37	8.72	8.27	8.52	8.56	8.52	7.81	8.25	7.53
Nd	33.71	35.37	36.05	36.67	36.75	36.51	36.45	36.07	36.32	37.15	36.56	33.85	40.36	32.92
Sm	7.30	7.66	7.52	7.52	7.84	7.44	8.24	7.60	7.76	7.80	7.89	7.89	8.74	7.73
Eu	2.43	2.50	2.66	2.68	2.67	2.63	2.56	2.47	2.72	2.75	2.75	2.29	2.42	2.14
Gd	6.45	6.78	6.73	6.78	6.82	6.79	7.98	7.84	6.96	7.27	6.79	7.54	8.02	7.18
Tb	0.91	1.07	0.98	1.01	1.02	0.99	1.19	1.22	0.97	1.04	1.02	1.18	1.13	1.16
Dy	5.11	5.33	5.53	5.46	5.47	5.77	7.13	6.87	5.50	5.31	5.59	6.69	6.90	6.43
Ho	0.94	0.97	0.97	1.02	1.02	0.98	1.37	1.33	1.03	1.09	1.05	1.28	1.28	1.25
Er	2.61	2.91	2.69	2.87	2.86	2.84	3.82	3.72	2.53	2.75	2.69	3.73	3.62	3.38
Tm	0.33	0.40	0.32	0.35	0.36	0.37	0.52	0.48	0.39	0.34	0.35	0.46	0.47	0.47
Yb	2.15	2.38	2.29	2.31	2.31	2.37	3.44	3.33	2.31	2.23	2.44	3.15	3.07	2.91
Lu	0.32	0.34	0.32	0.34	0.33	0.34	0.45	0.48	0.30	0.33	0.34	0.44	0.42	0.41
Hf	4.05	4.15	4.70	4.30	4.58	4.33	6.32	5.82	4.57	4.40	4.29	5.75	5.77	5.33
Ta	1.32	1.42	1.36	1.47	1.52	1.47	1.72	1.73	1.43	1.49	1.54	1.62	1.64	1.57
Pb	1.94	2.94	3.31	2.40	1.79	2.64	3.11	4.19	2.19	2.46	3.54	3.61	3.22	2.51
Th	2.88	3.04	2.99	3.06	3.11	3.07	4.73	4.24	3.04	3.03	2.97	4.09	4.20	3.93
U	0.71	0.78	0.76	0.78	0.82	0.79	1.21	1.06	0.78	0.78	0.77	1.02	1.05	0.97

LOI: Loss ion ignition, $mg = Mg^{2+}/(Mg^{2+}+Fe^{2+})$ in atomic ratio.

GXBGMR, 1985) suggested that these rocks are Hercynian layered mafic intrusions mainly composed of gabbro, diabase and olivine diabase that intruded the Paleozoic strata. However, Wu et al. (1993) argued that these rocks are late Paleozoic (early Carboniferous–early Permian) basaltic lava flows coeval with the enclosing deep-water silicalites, carbonates and tuffaceous flysch sedimentary rocks (Wu et al., 1993; Wang et al., 1997; Zhang et al., 1999). Our observations show that the mafic rocks in western Guangxi Province consist mainly of pillow basalts, olivine basalt and basaltic tuff (Fan et al., 2004), supporting an extrusive origin. The lavas occur either in the upper segment of the middle Permian Sidazhai Formation, or between the Permian Maokou Formation/pre-Permian limestone and upper Permian Longtan and Xuanwei Formations

20BS-90	20BS-91	20BS-92	20BS-93	20BS-94	20BS-97	20BS-98	20BS-99	20BS-100	20BS-102	20BS-104	20BS-105	20BS-106	20BS-107
Min'an area, Bama County													
46.35	44.85	46.01	46.22	45.85	45.67	45.38	45.72	44.73	45.98	45.80	45.65	45.76	46.14
3.10	3.08	3.04	3.07	3.01	2.97	2.59	3.01	2.57	3.00	3.00	3.07	3.06	3.05
13.52	14.20	13.92	13.78	13.70	13.99	14.68	13.74	13.42	13.87	13.90	13.80	13.81	13.66
5.63	5.42	5.45	5.91	6.01	5.84	6.75	5.93	8.10	5.85	5.83	5.86	5.84	5.88
3.49	3.68	2.65	2.24	2.14	2.06	2.46	2.56	2.42	1.98	2.40	1.91	2.75	2.36
10.43	10.20	10.70	11.57	11.55	11.60	10.43	11.40	11.77	11.70	11.50	11.92	11.27	11.30
9.48	11.32	10.72	9.58	10.19	10.20	9.75	9.83	9.55	10.07	9.95	10.11	10.10	9.78
0.89	1.09	1.12	1.26	1.12	1.15	1.09	1.27	1.22	1.24	1.14	1.13	0.93	1.18
2.56	2.49	2.74	2.04	2.80	2.75	2.65	2.71	2.16	2.70	2.80	2.74	2.82	2.83
0.56	0.33	0.51	0.56	0.55	0.55	0.48	0.56	0.44	0.56	0.55	0.55	0.57	0.56
0.22	0.19	0.21	0.23	0.23	0.22	0.21	0.23	0.22	0.22	0.21	0.24	0.23	0.22
3.50	2.77	2.65	3.25	2.60	2.74	3.26	2.79	3.15	2.58	2.66	2.75	2.60	2.78
99.73	99.72	99.72	99.71	99.75	99.74	99.73	99.75	99.75	99.75	99.74	99.73	99.74	99.74
0.43	0.42	0.43	0.44	0.45	0.44	0.49	0.44	0.51	0.44	0.43	0.44	0.43	0.44
73.6	69.1	90.9	71.8	71.2	73.6	126.2	72.2	163.8	70.4	75.0	74.3	79.4	82.4
77.8	69.9	59.8	86.8	72.6	76.0	100.2	72.4	132.5	72.9	74.4	70.8	75.4	77.6
5.5	23.0	22.6	25.1	23.9	23.6	25.7	28.2	27.9	28.0	27.8	29.2	25.5	29.9
589	560	581	610	575	588	606	541	525	562	529	510	529	521
30.92	18.86	26.19	27.38	26.25	26.15	23.36	26.32	21.58	26.43	27.39	26.83	26.25	28.71
150	95	139	146	147	142	134	148	122	150	150	152	149	156
24.61	14.67	23.48	24.25	23.37	23.26	20.81	24.11	20.45	24.72	24.38	24.36	24.15	25.22
0.16	1.73	3.04	0.83	3.43	3.34	5.23	4.29	4.32	4.15	2.29	2.66	2.87	2.25
440	468	543	723	527	461	531	539	538	603	600	551	397	626
30.51	18.36	27.90	29.76	28.87	28.61	26.82	30.61	24.56	30.89	30.59	30.89	28.08	29.83
68.19	42.56	63.89	67.26	66.16	65.49	59.66	68.43	55.57	70.26	70.23	68.46	67.04	66.91
8.53	5.37	7.66	8.35	8.19	7.87	7.38	8.26	6.87	8.68	8.69	8.65	7.97	8.45
36.96	24.16	34.37	36.49	35.42	34.59	32.11	37.86	30.49	38.28	37.33	37.08	35.07	36.74
8.10	5.44	7.59	7.71	7.90	8.00	6.60	8.01	6.10	8.69	7.44	8.04	7.42	8.00
2.65	2.01	2.61	2.62	2.60	2.71	2.39	2.84	2.27	2.74	2.70	2.95	2.67	2.69
7.10	4.98	6.63	7.14	7.31	7.08	6.14	7.02	5.63	7.15	7.01	7.37	6.56	7.00
1.07	0.74	0.99	1.05	0.99	0.96	0.87	1.02	0.83	1.11	1.07	1.01	0.92	1.00
5.80	4.13	5.55	5.60	5.54	5.50	5.08	5.64	4.62	5.89	5.90	5.91	5.36	5.72
1.06	0.74	0.95	1.04	1.02	0.99	0.85	1.04	0.83	1.03	1.00	1.05	0.98	1.02
2.85	1.94	2.79	2.78	2.63	2.69	2.48	2.87	2.32	2.83	2.83	2.75	2.49	2.88
0.38	0.26	0.35	0.38	0.39	0.36	0.34	0.34	0.31	0.37	0.37	0.39	0.38	0.35
2.50	1.62	2.23	2.39	2.32	2.38	2.09	2.27	1.86	2.33	2.41	2.23	2.12	2.25
0.33	0.26	0.31	0.33	0.32	0.30	0.29	0.33	0.27	0.35	0.32	0.36	0.27	0.29
4.53	3.03	4.18	4.53	4.34	4.16	4.03	4.42	3.66	4.34	4.30	4.35	3.93	4.27
1.53	0.97	1.39	1.51	1.47	1.47	1.22	1.49	1.20	1.53	1.57	1.58	1.40	1.42
2.54	2.16	2.85	2.18	3.11	3.14	2.94	3.31	2.54	3.41	1.96	2.82	2.44	2.01
3.12	1.86	2.99	3.06	3.01	2.94	2.78	3.12	2.62	3.25	3.23	3.10	2.73	2.84
0.81	0.44	0.79	0.80	0.74	0.74	0.76	0.82	0.63	0.83	0.81	0.84	0.72	0.72

(continued on next page)

or lower Triassic clastic strata (e.g., Fig. 1b; GXBGMR, 1985).

In the Yufeng area of Tianyang county, the basalts are >300 m thick and pseudo-conformably overlie middle–upper Carboniferous limestone. They, together with the middle–upper Carboniferous limestone, constitute the core of an anticline, the flanks of which are composed of the upper Permian Xuanwei Formation and mid–lower Triassic clastic rocks (Fig. 1b). The basaltic sequence is overlain unconformably by a 20-m-thick layer of conglomerate with interbedded bands of quartzite, and the whole package is overlain by a terrestrial, coal-bearing, clastic sequence with red mudstone interlayers. Most probably, the conglomerate and coal-bearing clastic sequence represent the basal unit of the Xuanwei Formation (late Permian). In the Yangxu section in Baise

Table 3 (*continued*)

Sample	20BS-110	20BS-111	20BS-112	20BS-113	20BS-114	20BS-115	20BS-116	20BS-117	20BS-118	20BS-119	20BS-120	20BS-121
Yufeng area, Tianyang County												
SiO_2	45.32	45.60	45.66	44.65	44.89	45.09	45.84	45.31	45.82	45.58	45.79	45.82
TiO_2	3.09	3.33	3.02	2.54	2.57	2.68	3.02	3.08	3.07	3.02	3.10	3.00
Al_2O_3	13.51	13.26	13.96	13.36	14.28	14.73	13.77	13.64	13.76	13.66	13.78	13.72
MgO	5.72	5.58	5.69	7.81	6.92	6.41	5.81	5.81	5.83	5.78	5.83	6.00
Fe_2O_3	1.80	1.70	1.43	2.12	2.09	2.51	2.34	2.64	2.15	1.60	2.72	2.16
FeO	11.87	12.20	12.23	12.00	11.10	10.07	11.36	11.13	11.73	12.17	10.93	11.57
CaO	10.10	10.69	9.88	9.53	10.26	10.48	9.83	9.96	9.60	10.22	9.86	9.79
K_2O	1.23	0.58	1.11	1.28	1.03	1.02	1.34	0.76	1.20	1.36	1.30	1.05
Na_2O	2.45	2.85	2.62	2.01	2.42	2.51	2.27	3.07	2.56	2.27	2.48	2.62
P_2O_5	0.54	0.57	0.55	0.46	0.46	0.48	0.55	0.56	0.55	0.55	0.56	0.56
MnO	0.23	0.22	0.22	0.23	0.20	0.20	0.23	0.22	0.24	0.24	0.23	0.20
LOI	3.39	3.14	3.36	3.76	3.53	3.55	3.39	3.60	3.23	3.30	3.12	3.24
Total	99.25	99.72	99.73	99.75	99.75	99.73	99.75	99.78	99.74	99.75	99.70	99.73
mg#	0.43	0.42	0.43	0.50	0.49	0.48	0.44	0.44	0.43	0.43	0.44	0.44
Cr	83.0	98.7	81.5	130.5	119.2	94.5	78.6	80.7	80.4	78.8	80.6	82.5
Ni	71.5	53.0	78.5	136.3	112.0	97.5	77.6	78.3	77.8	73.2	69.3	78.5
Rb	31.4	10.2	21.0	33.8	25.8	22.2	26.8	12.8	27.0	35.2	31.8	23.5
Sr	493	598	534	516	605	706	526	475	510	478	434	541
Y	25.86	27.53	26.88	22.07	22.86	23.18	26.79	27.50	28.06	25.91	28.54	28.20
Zr	149	159	156	127	128	130	151	151	154	149	152	153
Nb	23.72	25.45	25.07	20.58	21.20	20.97	24.54	24.05	24.21	23.85	24.58	24.62
Cs	22.04	7.09	3.50	11.22	9.59	6.13	10.99	1.63	5.93	13.84	8.26	6.45
Ba	557	465	527	510	414	567	573	389	567	551	733	483
La	27.43	29.43	29.57	23.70	24.08	24.67	29.02	28.89	29.06	28.07	29.98	29.14
Ce	61.86	66.52	66.40	53.75	54.71	55.06	65.63	64.45	65.79	62.73	68.05	65.79
Pr	7.71	8.28	8.17	6.77	6.72	6.84	8.11	7.96	8.17	7.94	8.40	8.20
Nd	34.64	36.54	35.81	29.58	30.19	30.68	35.78	35.58	36.80	35.48	36.59	35.95
Sm	7.52	7.76	7.59	6.39	6.49	6.41	7.90	7.77	7.57	7.26	7.84	7.65
Eu	2.57	2.60	2.65	2.28	2.30	2.42	2.63	2.70	2.65	2.56	2.77	2.61
Gd	6.55	6.94	7.06	5.66	5.84	5.87	6.95	6.82	6.91	6.78	7.32	6.72
Tb	0.97	1.04	1.00	0.80	0.83	0.79	0.96	0.93	1.00	0.94	0.98	0.99
Dy	5.37	5.82	5.63	4.55	4.66	4.65	5.55	5.51	5.84	5.33	5.84	5.62
Ho	0.98	1.01	0.99	0.77	0.83	0.84	0.96	1.04	1.02	0.98	1.05	1.02
Er	2.62	2.60	2.71	2.26	2.25	2.28	2.72	2.62	2.78	2.57	2.82	2.78
Tm	0.34	0.37	0.36	0.28	0.29	0.30	0.37	0.36	0.37	0.34	0.39	0.37
Yb	2.12	2.25	2.10	1.76	2.00	1.87	2.17	2.23	2.22	2.29	2.32	2.20
Lu	0.29	0.30	0.30	0.25	0.26	0.26	0.30	0.32	0.30	0.32	0.33	0.29
Hf	4.05	4.53	4.40	3.51	3.48	3.48	4.17	4.36	4.30	4.21	4.22	4.18
Ta	1.38	1.47	1.43	1.20	1.21	1.14	1.43	1.41	1.41	1.42	1.47	1.45
Pb	2.82	2.31	1.77	1.71	3.50	3.17	2.68	2.18	3.05	3.96	2.89	1.83
Th	2.66	2.90	2.88	2.29	2.36	2.30	2.84	2.76	2.85	2.72	2.78	2.73
U	0.68	0.75	0.74	0.57	0.62	0.59	0.72	0.70	0.76	0.69	0.72	0.72

County, the basaltic sequence pseudo-conformably overlies Permian/Carboniferous radiolarian-bearing cherts and carbonates (Wu et al., 1993). Numerous interlayered beds of basaltic tuff and pyroclastic breccia occur in the basal part of the sequence. Some cherts and claystones are intercalated with the volcanic rocks in the Yangxu section (Wu et al., 1993; Zhang et al., 1999; Wang et al., 1997). In the Min'an area of Bama County, the basaltic rocks overlie the early Permian Maokou Formation and are unconformably overlain by the upper Permian Longtan Formation/Xuanwei Formation or early Triassic clastic/ carbonate sedimentary rocks (GXBGMR, 1985; Fan et al., 2004) (Fig. 1b).

Sixty-five fresh samples were taken from the Yangxu, Yufeng and Min'an basaltic sections (Fig. 1b), 41 of which were selected for whole-rock geochemical analysis.

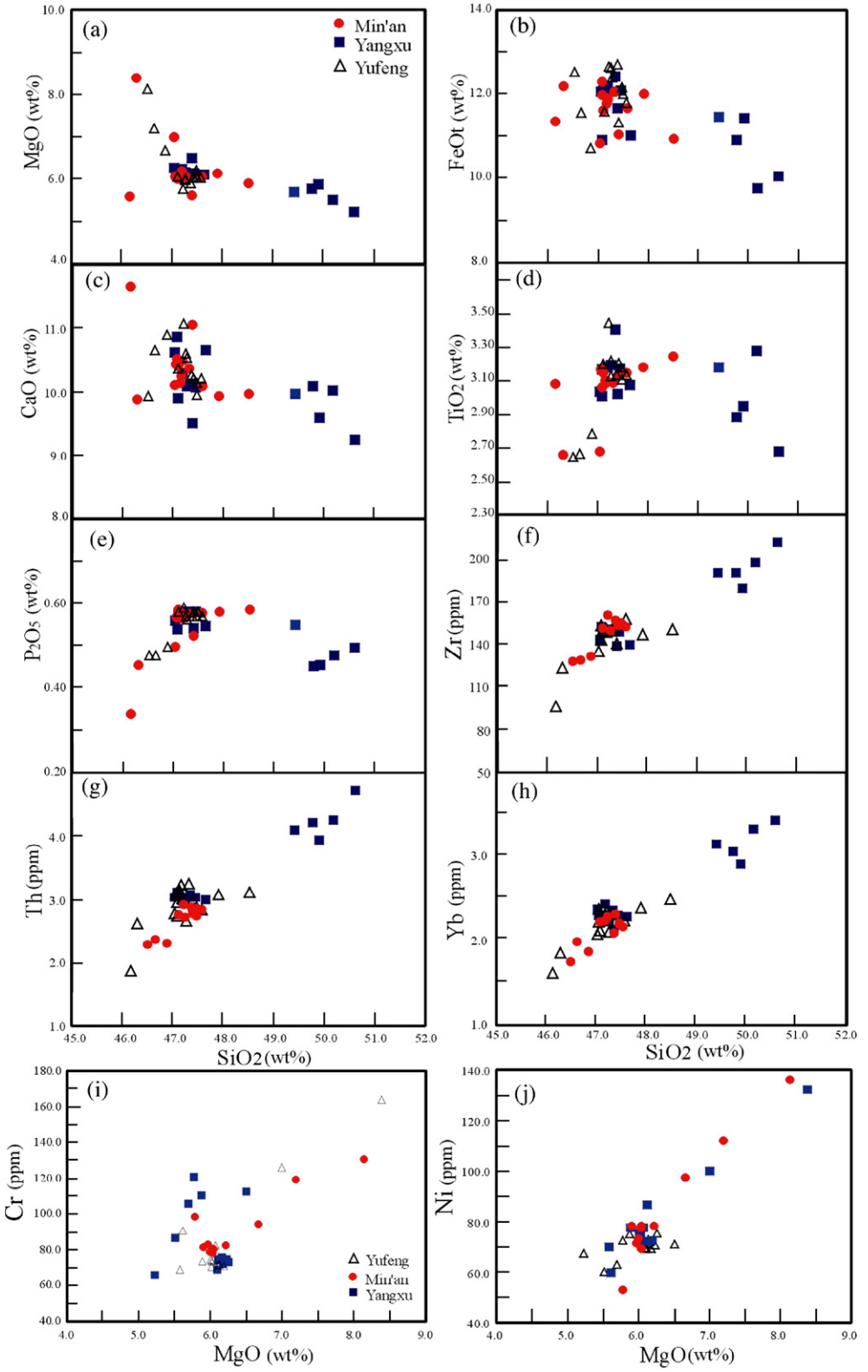

Fig. 3. Variations of SiO_2 versus (a) MgO, (b) FeOt, (c) CaO, (d) TiO_2, (e) P_2O_5, (f) Zr, (g) Th, (h) Yb, and MgO vs (i) Cr and (j) Ni for the Permian basalts in western Guangxi Province. All major oxides are normalized to 100% on a volatile-free basis. Symbols are the same as those in Fig. 3a.

All of the samples are fine-grained, moderately phyric, massive basalts with phenocrysts of plagioclase (5–15 modal %), clinopyroxene (5–10 modal%) and olivine (5–7 modal %). The groundmass consists of fine-grained to aphanitic plagioclase (20–40 modal%), clinopyroxene (8–20 modal%), quartz (1–2 modal%), amphibole (1–5 modal%), biotite (1–5 modal%) and opaque oxides.

3. Analytical methods

Zircons were separated by conventional heavy liquid and magnetic techniques, and were then handpicked under a binocular microscope. The separates were mounted in epoxy, polished and coated with gold. The mounts were then photographed in transmitted and reflected light, and the cathodoluminescence images were obtained on a scanning electron microscope. U–Pb isotopic determinations were undertaken using the sensitive high-resolution ion microprobe (SHRIMP II) at the Beijing SHRIMP Center (CAS). A spot size in the range of 25–30 μm was used for data collection and, before each analysis, the spot was rastered over 120 μm for five minutes to remove any common Pb on the surface. Detailed analytical procedures for the SHRIMP analyses are described in Song et al. (2002) and Williams and Claesson (1987). The calculation of $^{206}Pb/^{238}U$ ages is based on the assumption that the bias in the measured $^{206}Pb/^{238}U^{+}$ ratio can be described by the same power law relationship between $^{206}Pb/^{238}U^{+}$ and UO^{+}/U^{+} for the analytical standard and samples (Compston et al., 1984; Williams and Claesson, 1987; Song et al., 2002). The standard TEM zircon of RSES (age=417 Ma) was used to determine the elemental discrimination that occurs during sputter ionization. Common Pb correction was made using the observed ^{204}Pb peak (Compston et al., 1984). Data processing of the analytical results was carried out using the Isoplot programs of Ludwig (2001).

For whole-rock geochemical analyses the samples were crushed to 200-mesh using an agate mill. Major elements were determined by X-ray fluorescence (XRF) spectrometry at the Hubei Institute of Geology and Mineral Resources. Total iron was determined by XRF, and FeO contents were determined by wet chemical methods. Trace element analyses were performed at the Institute of Geochemistry, the Chinese of Academy Sciences (CAS) using inductively coupled plasma mass spectrometry (ICP-MS). About 100-mg samples were digested with 1 ml of HF and 0.5 ml HNO_3 in screw top PTFE-lines stainless steel bombs at 190 °C for 12 h. Sample preparation and analytical procedures followed Qi et al. (2000). Based on repetitive analyses of BHV-1 and AMH-1 standards, the reproducibility was better than 95% and the analytical error was less than 5% for elements present in amounts >10 ppm, less than 8% for those present in amounts <10 ppm, and about 10% for transition metals.

Analyses of Sr and Nd isotopic ratios were performed on the VG-354 mass-spectrometer at the Institute of Geophysics and Geology (IGG, CAS). The total procedural blanks were in the range of 200 to 500 pg for Sr and ≤50 pg for Nd. The mass fractionation corrections for isotopic ratios are based on $^{86}Sr/^{88}Sr=0.1194$ and $^{146}Nd/^{144}Nd=0.7219$, respectively. The measured $^{87}Sr/^{86}Sr$ ratio of the (NIST) SRM 987 standard and $^{143}Nd/^{144}Nd$ ratio of the La Jolla standard were 0.710265±12 (2σ) and 0.511862±10 (2σ), respectively. $^{87}Rb/^{86}Sr$ and $^{147}Sm/^{144}Nd$ ratios were calculated using the Rb, Sr, Sm and Nd abundances measured by ICP-MS. Pb isotopes were extracted using HBr and HCl anion microcolumn procedures, and the purified Pb was loaded on Re single filaments with silica gel and phosphoric acid. Pb isotopic ratios were measured at the IGG, using a VG-354 mass spectrometer. Repeated analyses of NBS 981 yielded average values of $^{206}Pb/^{204}Pb=16.942\pm4$ (2σ), $^{207}Pb/^{204}Pb=15.498\pm4$ (2σ) and $^{208}Pb/^{204}Pb=36.728\pm9$ (2σ). External precisions are estimated to be better than 0.005, 0.005 and 0.0015, respectively.

4. Results

4.1. SHRIMP zircon U–Pb geochronology

Two porphyritic basalts were collected in western Guangxi Province for zircon separation, one from Min'an (20BS-116, Bama County) and the other from Yangxu (20BS-76, Baise County) (Fig. 1b). They are composed of clinopyroxene (20–25 modal%), plagioclase (43–50 modal%), amphibole (~3–5 modal%), biotite (~3%), quartz (1–2 modal%) and minor amounts of Fe–Ti oxides, zircon, titanite and apatite. Some of the separated zircons are euhedral, transparent and light brown, and exhibit cathodoluminescence images of typical magmatic zircons, whereas others are irregular and transparent, perhaps broken fragments, with insignificant internal structures (Fig. 2a). Several zircon grains have cores surrounded by heterogeneously spotted rims, similar to inherited zircons.

The SHRIMP U–Pb analytical results for these zircons are listed in Tables 1 and 2, and the cathodoluminescence images of the representative zircons are shown in Fig. 2a. For sample 20BS-116, two grains (A13.1 and A14.1) with

the lowest U and Th contents yield $^{206}Pb/^{238}U$ apparent ages of 716 Ma and 2263 Ma, respectively. Fourteen other grains have high Th and U contents and relatively constant Th/U ratios (Table 1). These analyses form a single-age population with $^{206}Pb/^{238}U$ apparent ages of 244–271 Ma and yield a weighted mean $^{206}Pb/^{238}U$ age of 259.6±5.9 Ma with MSWD=1.3 (Fig. 2b). This age is taken as the best estimate of the formation age for the Bama basalts.

Four grains (E1.1, E2.1, E7.1 and E13.1) from sample 20BS-76, which exhibit cathodoluminescence images of inherited zircon and give $^{206}Pb/^{238}U$ apparent ages of 913 Ma, 456 Ma, 1276 Ma and 492 Ma,, respectively (Table 2), likely represent xenocrysts from a crustal source. Three other grains with cracks and liquid–gas inclusions (E8.1, E9.1 and E14.1) yield younger $^{206}Pb/^{238}U$ apparent ages of 223 Ma, 234 Ma and 225 Ma, respectively. The remaining seven grains (E3.1, E4.1, E5.1, E6.1, E10.1, E11.1 and E12.1) yield an age-population group with a weighted mean $^{206}Pb/^{238}U$ age of 259.1±4.0 Ma (MSWD=0.85, Fig. 2c).

4.2. Geochemical characteristics

All of the basalts have a narrow compositional range in major oxides: SiO_2=46.17–50.61 wt.% (volatile-free to 100%), FeOt=11.86–14.71 wt.%, and P_2O_5=0.34–0.59 wt.% (Table 2). Titania ranges from 2.65 to 3.45 wt.% (Table 3), similar to the Emeishan high-Ti basalt defined by Xu et al. (2001), and MgO ranges from 5.22 to 8.39% giving *mg*-numbers (=Mg/(Mg+∑Fe) of 0.42–0.51, indicative of an evolved magma. The samples from the Yangxu section are generally more evolved than those of the Yufeng and Min'an sections, as reflected by higher SiO_2 contents. Total alkalis (Na_2O+K_2O) lie in the range of 3.42–4.14 wt.% and the rocks have K_2O/Na_2O ratios of 0.20–0.65. Cr and Ni contents vary from 66 to 166 ppm and 53 to 136 ppm, respectively.

Negative correlations are seen between SiO_2 and MgO, FeOt and CaO in the Harker diagrams (Fig. 3a–c), but there is no clear correlation between SiO_2 and Al_2O_3 (not shown). In the Harker diagrams, TiO_2 and P_2O_5 show a positive correlation with silica up to 49 wt.% SiO_2, and then decrease with further fractionation (Fig. 3d–e). All of the immobile trace elements (e.g., Th, REE, Nb, Ta, Zr and Hf) correlate positively with SiO_2 contents (Fig. 3f–g), whereas Cr and Ni correlate positively with MgO (Fig. 3i–j). All of the samples plot along the boundary between sub-alkaline and alkaline basalts in the major oxide and Nb/Y vs Zr/Ti diagrams (Fig. 4a–b).

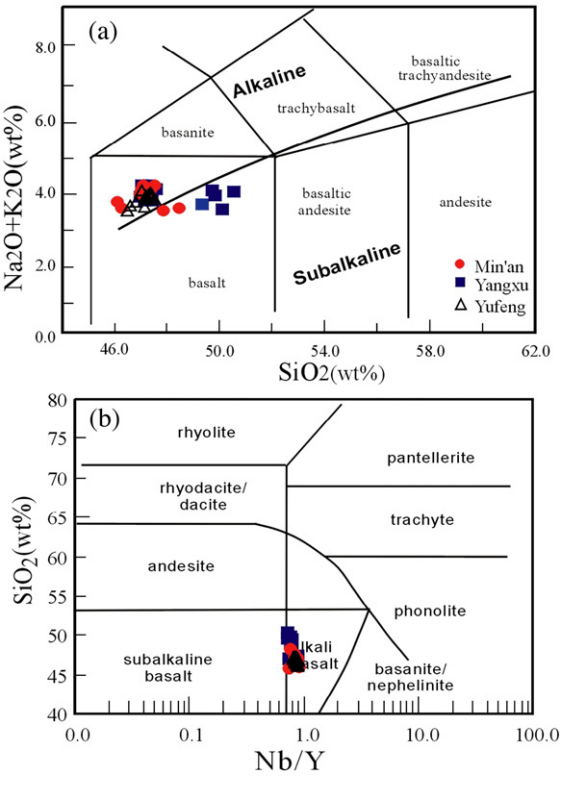

Fig. 4. (a) SiO_2 versus K_2O+Na_2O (after LeBas et al., 1986), and (b) Nb/Y versus SiO_2 (after Winchester and Floyd, 1977) for the Permian basalts in western Guangxi Province. Symbols in (b) are the same as in (a).

Chrondrite-normalized REE patterns of these samples all show LREE enrichment (Fig. 5a–c), and are sub-parallel to those of the Emeishan high-Ti basalts (Xu et al., 2001; Xiao et al., 2003, 20004a,b; Zhou et al., 2006). The analysed samples have (La/Yb)cn ranging from 6.40 to 10.09 and (Gd/Yb)cn from 1.92 to 2.78 and show both slightly positive and negative europium anomalies with Eu/Eu* values ranging from 0.86 to 1.18. (Nb/La)n and (Hf/Sm)n ratios range from 0.75 to 0.94 and 0.78 to 0.90, respectively. Several other key parameters are: Ba/Nb=12.0–49.2, Ce/Pb=15.6–37.9, Nb/U=23.0–36.1 and Th/La=0.09–0.15. On primitive mantle-normalized spidergrams (Fig. 5d–f), the samples exhibit enrichment in LILE, and again have patterns similar to those of the Emeishan high-Ti basalts (Zhou et al., 2006; Xiao et al., 2003, 2004a,b; Xu et al., 2001). These basalts are all lower in Nb, Ta, Zr and Hf than ocean island basalts (Sun and McDonough, 1989).

The initial Sr isotopic ratios of these samples vary from 0.704922 to 0.705804, and $\varepsilon_{Nd}(t)$ values range from −0.23 to+1.50, both being similar to those of the

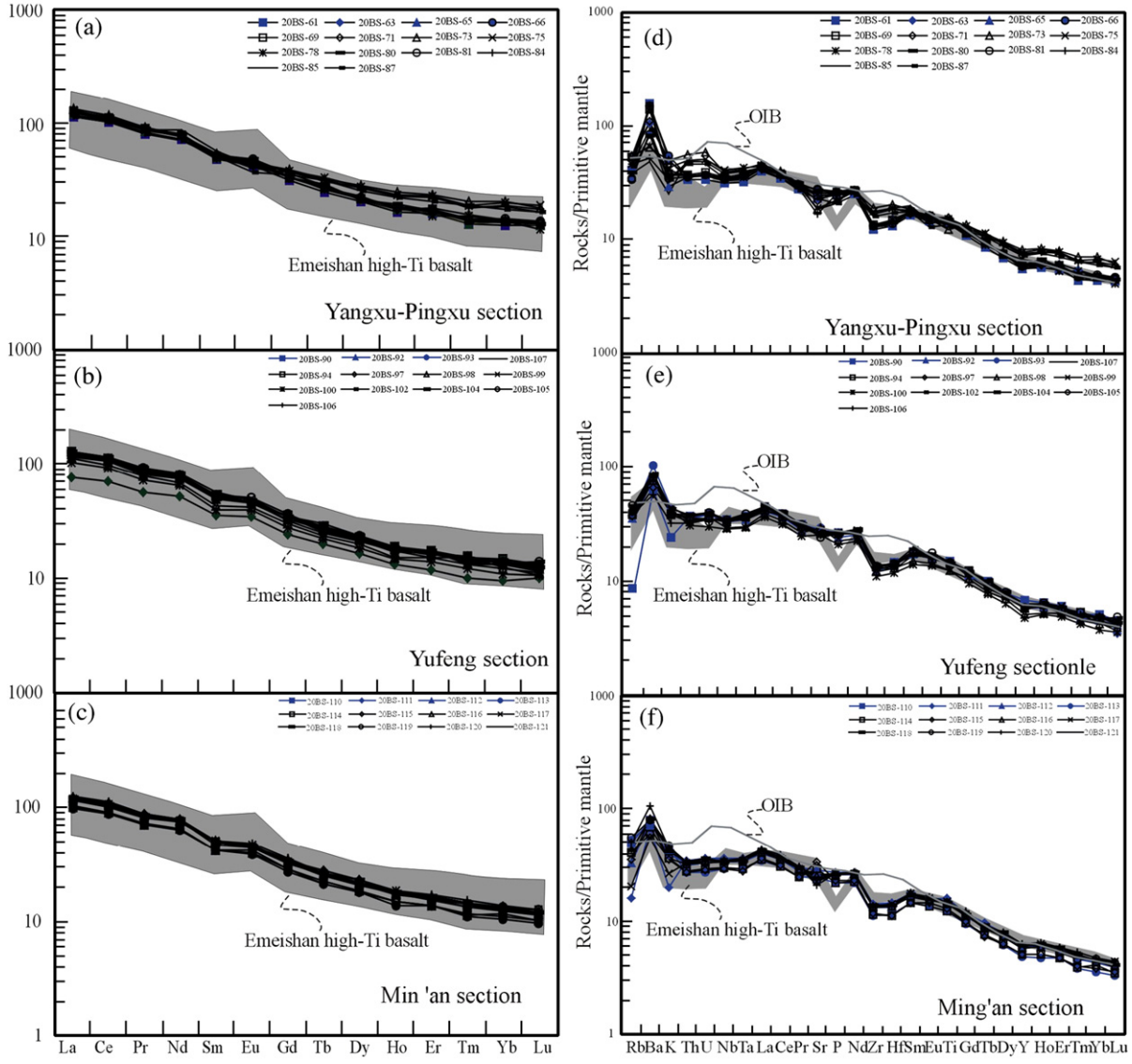

Fig. 5. Chondrite-normalized REE patterns for the Permian basalts in western Guangxi Province (a), Yangxu–Pingxu profile; (b), Yufeng profile; (c), Ming'an profile) and primitive mantle-normalized trace element patterns for the same samples (d), Yangxu–Pingxu profile; (e), Yufeng profile; Ming'an profile). Chrondrite normalizing values are from Taylor and McLennan (1985) and primitive mantle values are after Sun and McDonough (1989). Shaded data are for the Emeishan high-Ti basalts (Xu et al., 2001; Xiao et al., 2003; Zhou et al., 2006).

Emeishan high-Ti basalts (Table 4 and Fig. 6; Xu et al., 2001; Xiao et al., 2003, 2004a,b; Zhou et al., 2006). T_{DM} values vary from 0.98 Ga to 1.26 Ga. Based on our Pb isotopic determinations, these samples have prominent positive Δ8/4 (67.7–82.7) and slightly positive Δ7/4 (0.96–8.19) values with $(^{206}Pb/^{204}Pb)_i$ ratios of 18.77–19.67, $(^{207}Pb/^{204}Pb)_i$ ratios of 15.55–15.67 and $(^{208}Pb/^{204}Pb)_i$ ratios of 39.02–40.20 (Table 3). These data overlap with the isotopic composition of OIB, and plot above the low Nd (LoNd) array (Hart, 1984; Hart et al., 1986) in the $(^{206}Pb/^{204}Pb)_i$ vs $(^{87}Sr/^{86}Sr)_i$ plot (Fig. 7a). In the $(^{206}Pb/^{204}Pb)_i$ vs $(^{207}Pb/^{204}Pb)_i$ diagram (Fig. 7b), the samples plot above the North Hemisphere Reference Line (NHRL) and around the LoNd array (Hart, 1984, 1988; Hart et al., 1986), and show a linear trend between HIMU and EM1 components. In Fig. 7c, these data define a linear array and plot above the NHRL and LoNd array. The Pb isotopic compositions for these

Table 4
Sr, Nd and Pb isotopic compositions of Permian basalts from western Guangxi Province, SW China

Sample	Sm	Nd	Rb	Sr	$^{147}Sm/^{144}Nd$	$^{143}Nd/^{144}Nd \pm 2\sigma$	$^{87}Rb/^{86}Sr$	$^{87}Sr/^{86}Sr \pm 2\sigma$	$(^{87}Sr/^{86}Sr)i$	$\varepsilon_{Nd}(t)$	$^{238}U/^{204}Pb$	$^{232}Th/^{204}Pb$	$^{206}Pb/^{204}Pb$	$^{207}Pb/^{204}Pb$	$^{208}Pb/^{204}Pb$	$(^{206}Pb/^{204}Pb)i$	$(^{207}Pb/^{204}Pb)i$	$(^{208}Pb/^{04}Pb)i$	Δ7/4	Δ8/4
20BS-61	7.30	33.71	25.66	480.6	0.131	0.512571±8	0.155	0.706092±15	0.705519	0.88	178.52	272.79	19.316	15.590	39.616	19.244	15.587	39.581	0.96	68.79
20BS-71	7.44	36.51	31.11	460.8	0.123	0.512569±9	0.196	0.706204±16	0.705480	1.09	218.58	263.13	19.207	15.606	39.483	19.119	15.602	39.449	3.85	70.75
20BS-75	7.60	36.07	33.54	392.9	0.127	0.512597±6	0.247	0.706092±18	0.705177	1.50	262.13	274.41	19.772	15.641	40.240	19.666	15.636	40.205	1.33	80.12
20BS-78	7.759	36.323	29.30	531.81	0.129	0.512553±10	0.160	0.706199±20	0.705608	0.58										
20BS-80	7.803	37.153	24.67	571.03	0.127	0.512557±8	0.125	0.705514±16	0.705050	0.73										
20BS-84	7.89	33.85	29.43	354.3	0.141	0.512572±8	0.241	0.706098±18	0.705207	0.56	230.76	270.33	19.331	15.644	39.738	19.238	15.640	39.703	6.33	81.76
20BS-85	8.74	40.36	24.16	383.0	0.131	0.512570±6	0.183	0.706430±18	0.705754	0.86	199.82	269.59	19.323	15.612	39.603	19.242	15.608	39.568	3.14	67.73
20BS-92	7.59	34.37	22.56	580.7	0.134	0.512599±8	0.113	0.706220±13	0.705804	1.34	232.16	252.28	19.072	15.575	39.299	18.978	15.571	39.267	2.24	69.47
20BS-97	8.00	34.59	23.57	587.6	0.140	0.512540±9	0.116	0.705676±19	0.705246	−0.02	273.54	264.66	18.885	15.554	39.058	18.775	15.549	39.024	2.27	69.84
20BS-99	8.007	37.856	28.23	541.5	0.128	0.512588±12	0.151	0.705197±20	0.704638	1.31										
20BS-100	6.10	30.49	27.89	525.0	0.121	0.512553±7	0.154	0.705881±18	0.705311	085	260.37	276.98	19.066	15.602	39.389	18.961	15.597	39.353	5.08	80.26
20BS-102	8.69	38.28	27.96	561.9	0.137	0.512549±8	0.144	0.705716±17	0.705182	0.24										
20BS-106	7.42	35.07	25.46	529.3	0.128	0.512579±8	0.139	0.705492±15	0.704976	1.13	222.99	258.41	19.588	15.678	39.973	19.498	15.674	39.940	6.93	73.96
20BS-110	7.52	34.64	31.36	492.7	0.131	0.512562±8	0.185	0.705605±20	0.704922	0.69										
20BS-113	6.39	29.58	33.81	516.1	0.131	0.512560±9	0.190	0.705676±18	0.704974	0.67	196.55	271.33	19.373	15.636	39.729	19.294	15.632	39.694	4.99	74.10
20BS-115	6.41	30.68	22.20	706.1	0.126	0.512537±7	0.091	0.705531±18	0.705194	0.36	347.10	259.73	19.039	15.628	39.336	18.899	15.622	39.303	8.19	82.67
20BS-117	7.768	35.58	12.80	474.74	0.132	0.512516±9	0.078	0.705345±15	0.705056	−0.23										
20BS-119	7.261	35.483	35.24	478.4	0.124	0.512560±10	0.214	0.705348±16	0.704558	0.90										
20BS-121	7.65	35.95	23.49	541.4	0.129	0.512543±8	0.126	0.705767±18	0.705302	0.40										

Chondrite uniform reservoir values, $^{147}Sm/^{144}Nd = 0.1967$, $^{143}Nd/^{144}Nd = 0.512638$, are used for the calculation. $\varepsilon_{Nd}(t)$ is calculated by assuming 260 Ma. Sm, Nd, Rb, and Sr: ppm. $\lambda_{U238} = 1.55125 * 10^{-10}$/year, $\lambda_{U235} = 9.848 * 10^{-10}$/year, $\lambda_{Th232} = 4.9475 * 10^{-11}$/year (Steiger and Jäger, 1977). Initial Pb isotopic ratios were calculated using the measured whole-rock Pb isotopic compositions, whole-rock U, Th and Pb contents (ICP-MS result in Table 2) by assuming 260 Ma. $\Delta 7/4 = ((^{207}Pb/^{204}Pb)_i - (^{207}Pb/^{204}Pb)_{NHRL}) * 100$; $\Delta 8/4 = ((^{208}Pb/^{204}Pb)_i - (^{208}Pb/^{204}Pb)_{NHRL}) * 100$; $(^{207}Pb/^{204}Pb)_{NHRL} = 0.1084 * (^{206}Pb/^{204}Pb)_i + 13.491$, $(^{208}Pb/^{204}Pb)_{NHRL} = 1.209 * (^{206}Pb/^{204}Pb)_i + 15.627$ (Hart, 1984).

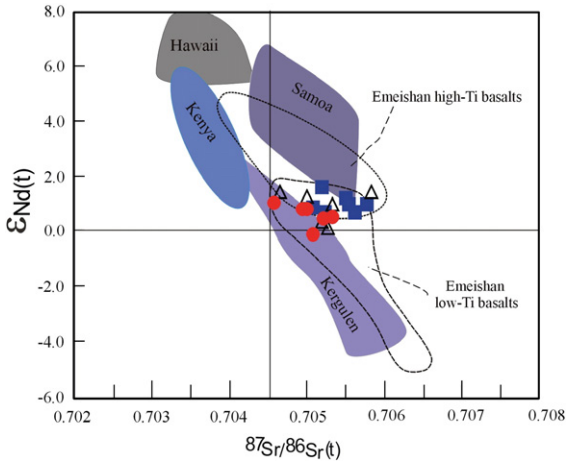

Fig. 6. Initial $^{87}Sr/^{86}Sr(t)$ versus $\varepsilon_{Nd}(t)$ (t=260 Ma) diagram for the Permian basalts in western Guangxi Province. The fields for Hawaii, Kenya, Kergulen, and Samoa are from Hawkesworth et al. (1984), Hart (1988) and Weaver (1991). The ranges of Emeishan high- and low-Ti basalts are from Xu et al. (2001), Zhou et al. (2006) and Xiao et al. (2003, 2004a,b).

basaltic rocks are closer to Indian Ocean MORB and Kerguelen lavas than to the HIMU component (Hart, 1984, 1988; Hamelin and Allègre, 1985; Hart et al., 1986; Barling and Goldstein, 1990; Deniel, 1998).

5. Discussion

5.1. Petrogenesis

5.1.1. Magma processes

The samples have loss on ignition (LOI) of 2.57–4.20 wt.%, and their Ba/Rb and K_2O/P_2O_5 ratios range from 12.4 to 49.3, 1.0 to 3.3, respectively. The Rb/Sr ratios generally increase with increasing of K_2O/P_2O_5 ratios and K_2O+Na_2O decreases with increasing of LOI (Fig. 8a–b). No significant correlations are observed between Rb and Zr (Fig. 8c), however, there is a clear positive correlation between Th and Zr (Fig. 8d). These geochemical features, together with the consistency of the dataset in Fig. 5a–f, suggest that the highly incompatible elements (e.g., Rb, Ba and K) for the samples might have been mobile but that the moderately incompatible elements (e.g. Zr, Th, Hf and LREE) were immobile during low-temperature alteration (Frey et al., 1994; Roden et al., 1994; Hollanda et al., 2006).

The low Ni and Cr contents and *mg*-numbers for these samples suggest that they have undergone considerable crystal fractionation. The generally positive correlations between SiO_2 and other major oxides and the decrease in Ni and Cr with decreasing MgO (e.g., Fig. 3a–c and i–j) indicate fractionation of olivine and clinopyroxene. The positive correlation between SiO_2 and P_2O_5 and TiO_2 up to 49 wt.% SiO_2 (Fig. 3d–e) argue against early fractionation of apatite and Ti–Fe-oxides. Considering the small depletions of P and Ti as shown in Fig. 5d–f, fractionation of apatite and Ti–Fe-oxides fractionation might be insignificant in the evolution of these magmas. Because Sr is compatible in plagioclase, the increasing Sr content with increasing SiO_2 and the lack of negative Sr and Eu anomalies for these samples argue against significant fractionation of plagioclase. The linear correlation between SiO_2 and the moderately incompatible trace elements, such as Nb, Ta, Zr and Hf (Fig. 3f–h) indicate that the abundances of these elements were most likely related to partial melting rather than crystal

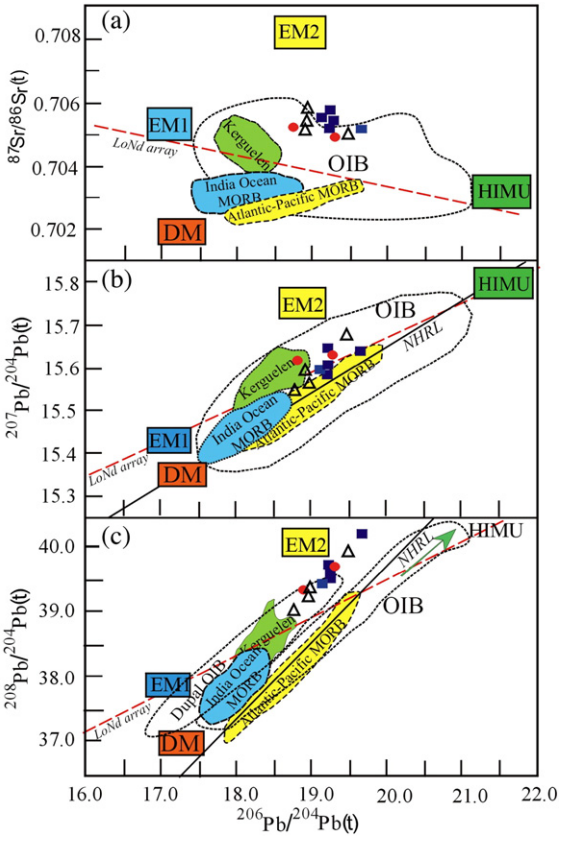

Fig. 7. Plots of $^{206}Pb/^{204}Pb$ vs $^{87}Sr/^{86}Sr$ (a), $^{207}Pb/^{204}Pb$ (b), and $^{208}Pb/^{204}Pb$ (c) for the Permian basalts in western Guangxi Province. These samples display a mixing trend between HIMU and EM1 components. The field of HIMU, OIB, Dupal OIB, EM1 and EM2 are from Hawkesworth et al. (1984), Hart (1984, 1988), Hamelin and Allègre (1985), Hart et al. (1986) and Weaver (1991). The LoNd array and Northern Hemisphere Reference Line (NHRL) are from Hart (1984). The fields of Indian Ocean MORB, Atlantic–Pacific MORB and Kerguelen are from Hamelin and Allègre (1985), Barling and Goldstein (1990), Deniel (1998) and references therein.

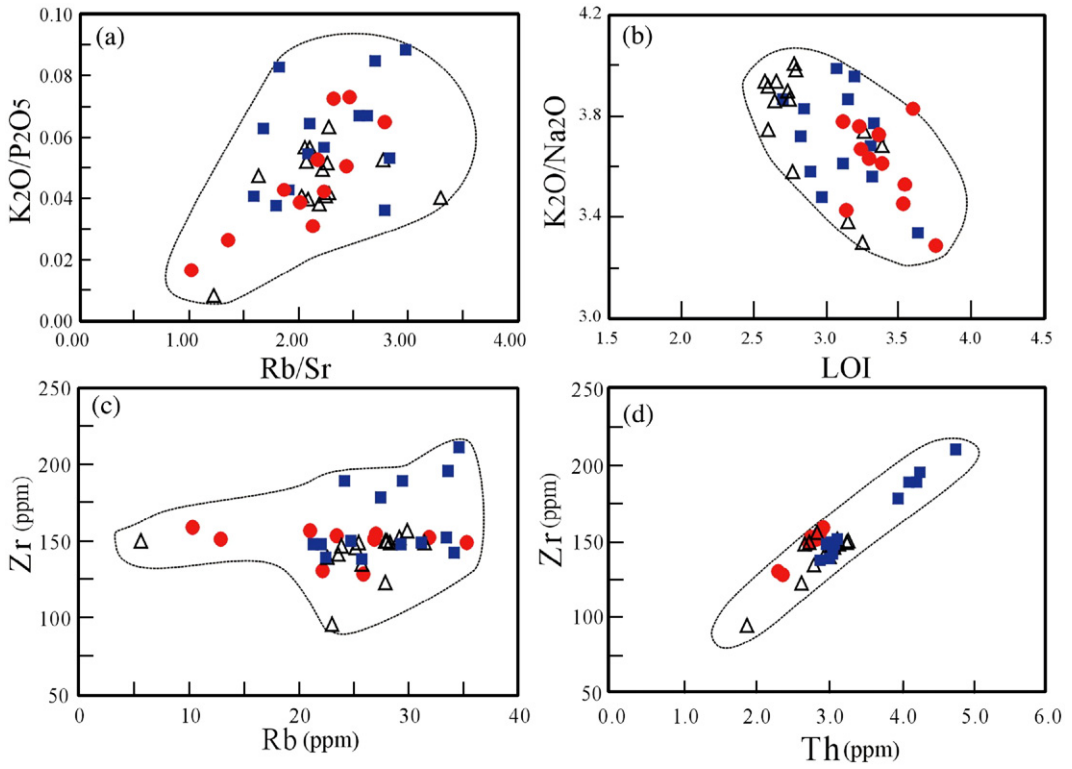

Fig. 8. Plots of (a) Rb/Sr vs K_2O/P_2O_5, (b) LOI (loss on ignition) vs K_2O/Na_2O, (c) Zr vs Rb and (d) Zr vs Th for the Permian basalts in western Guangxi Province. These plots suggest that the mobile elements were significantly modified by post-magmatic alteration whereas the immobile elements were little affected. Symbols are the same as those in Fig. 3a.

fractionation because they would have been little affected by fractionation of olivine and clinopyroxene.

Elevated SiO_2 contents, high $^{87}Sr/^{86}Sr$ ratios, low $\varepsilon_{Nd}(t)$ values and negative Nb and Ta anomalies are commonly used as indicators of crustal contamination of mafic melts (e.g., DePaolo, 1981). The basaltic rocks in western Guangxi exhibit a weak correlation between SiO_2 (and TiO_2) and Sr, Nd and Pb isotopic compositions (Fig. 9a). The basalts with high SiO_2 (e.g., 20BS-85) have higher $\varepsilon_{Nd}(t)$ values than those with low SiO_2 (e.g., 20BS-115). Nb/La ratios increase with increasing SiO_2 (Fig. 9b), and $\varepsilon_{Nd}(t)$ values decrease with increasing $^{147}Sm/^{144}Nd$ ratios (Fig. 9c). All of the samples have high Nb/La ratios and TiO_2 contents. Such geochemical signatures do not support crustal assimilation or AFC processes (e.g., DePaolo, 1981). Sr/Ce ratios range from 5.5 to 9.6, overlapping those of ocean island basalts (~5–8). $(Th/La)_N$ is 0.75–0.86 and $(U/La)_N$ is 0.78–0.90, varying slightly irrespective of SiO_2 content. Several samples with SiO_2>49% have higher $(Th/La)_N$ ratios, but they also exhibit higher Nb/La ratios and $\varepsilon_{Nd}(t)$ values than the others. The observed variability of elemental and isotopic compositions in these rocks is much more likely to be related to magma source regions rather than crustal assimilation. Xu et al. (2001) and Zhou et al. (2006) also proposed that the Emeishan high-Ti basalts were some of the least contaminated lavas in the LIP (e.g., Song et al., 2001; Xiao et al., 2004a,b).

5.1.2. Plume-lithosphere interaction

In the Zr/Nb and Ce/Y diagram (Deniel, 1998), the Guangxi basaltic rocks plot in the field of a melting column across the garnet–spinel lherzolite transition. The high La/Sm (3.36–4.11) and Sm/Yb (2.28–3.73) ratios, similar to those of Reunion (Lassiter and DePaolo, 1997) and the Emeishan basalts in Binchuan (Xiao et al., 2004a,b), indicate derivation by low degrees of melting of a garnet-bearing mantle source. This interpretation is supported by the high LREE, TiO_2, and P_2O_5 contents, the high La/Yb ratios and the relatively low HREE concentrations of these samples (cf., Deniel, 1998; Xu et al., 2001; Zhou et al., 2006). The most evolved samples have higher Zr/Nb and HREE, and lower Ce/Y, La/Yb and Sm/Yb ratios, indicating higher degrees of melting and shallower depths of formation than the less evolved samples.

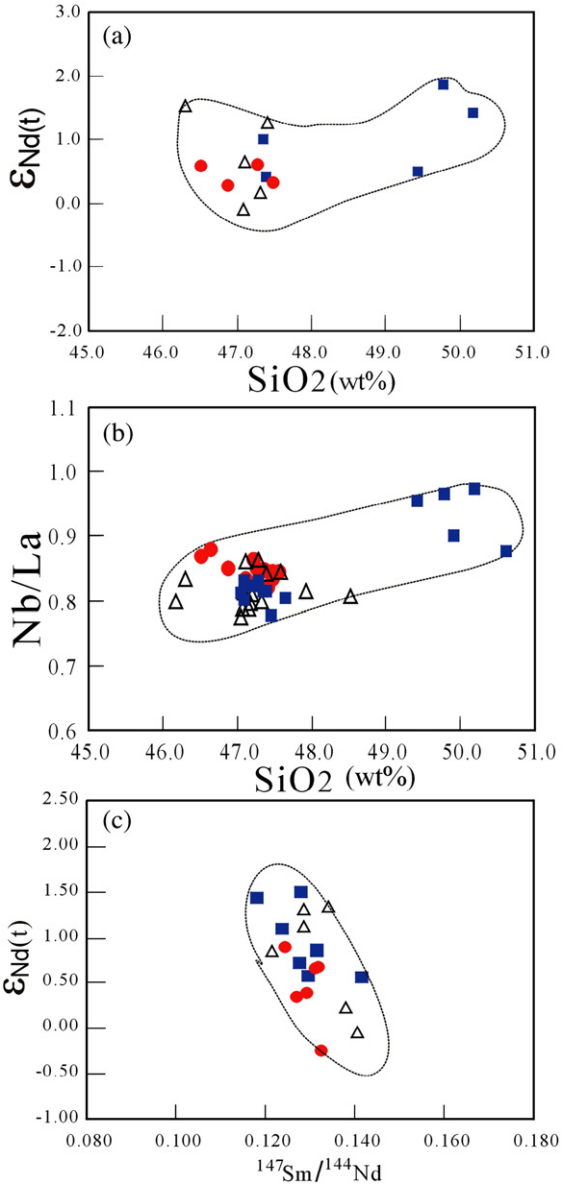

Fig. 9. (a) SiO_2 versus $\varepsilon_{Nd}(t)$, (b) SiO_2 versus Nb/La, and (c) $^{147}Sm/^{144}Nd$ vs $\varepsilon_{Nd}(t)$ for the Permian basalts in western Guangxi Province. Symbols are the same as those in Fig. 3a.

The variations of LILE and HFSE abundances of these samples could be interpreted as the result of variable partial melting of the mantle source. However, Sr–Nd–Pb isotopic compositions and the ratios of highly incompatible elements with similar bulk distribution coefficients (e.g. Th/La, Zr/Nb, Ce/Pb and Nb/U) are little affected by degrees of partial melting or crystal fractionation. The samples in western Guangxi samples have Ce/Pb ratios of 15.6–37.8, Nb/U ratios of 23.0–36.1 and Th/La ratios of 0.09–0.15. Nb/Th ratios vary from 5.9 to 9.1. These compositional ranges most likely reflect derivation from a heterogeneous mantle source. The correlation between $\varepsilon_{Nd}(t)$ values and (La/Yb)cn ratios for these rocks (Fig. 10a) argues against generation by variable degrees of partial melting of a homogeneous source. The possibility of source variability is also supported by the negative correlations between Yb and La/Yb (and Tb/Yb) ratios (Fig. 10b).

Ce/Pb, Nb/U and Th/La ratios for most samples fall near or within the ranges for OIB (Hofmann et al., 1986; Sun and McDonough, 1989; Weaver, 1991), similar to those of high-Ti basalts in the Binchuan section, SW China (e.g., Xu et al., 2001; Xiao et al., 2004a,b). Nb/Th ratios are close to that estimated for OIB (Sun and McDonough, 1989). These samples show similar trace element patterns to OIB with the exception of lower Nb and Ta contents and negative Zr–Hf anomalies. The OIB-like geochemical signatures are also indicated by the high LILE/LREE and LREE/HFSE ratios described above. As shown in Fig. 7a–c, the Pb isotopic compositions for these samples tend to cluster near/toward the estimated HIMU-type OIB source (Hart, 1984, 1988, Hart et al., 1986; Weaver, 1991). The extremely high Pb isotopic compositions for several samples (e.g., $^{206}Pb/^{204}Pb = 19.5$ for 20BS-106) are close to the HIMU-type reservoir characterized by a high $^{206}Pb/^{204}Pb$ ratio of 20.5 (Hart, 1988). These characteristics, together with the enrichment in alkalis and highly incompatible trace elements and moderate depletion in Nd isotopic ratios, suggest a potential HIMU-type component in the magma source. Xiao et al. (2004a,b) also considered that the geochemical signatures of the high-Ti basalts in the Binchuan section, SW China are similar to other flood basalts (e.g. Ethiopian; northern Karoo) with a plume origin.

However, as illustrated in Fig. 10c–d, the western Guangxi samples define a linear array that can be attributed to binary mixing. The trends on Sr–Nd–Pb isotopic diagrams also strongly support an origin of binary mixing between an end-member akin to a HIMU-type source and another end-member component (Figs. 7 and 10d). These basalts have higher La/Nb and Ba/La ratios, and Nb (–Ta) contents than the estimated OIB-type source. In primitive mantle- normalized incompatible element patterns (Fig. 5d–f), the western Guangxi samples display negative Nb and Ta anomalies, indicative of an affinity to arc basalts. Most samples have $^{87}Sr/^{86}Sr$ ratios of ~0.7050 and $\varepsilon_{Nd}(t)$ values of ~+1. Pb isotopic compositions plot above the NHRL, and are similar to the southern Hemispheres component (e.g., Duprè and Allègre, 1983; Hart, 1984, 1988; Hart et al., 1986). Such elemental and isotopic signatures could be due to the involvement of a subcontinental

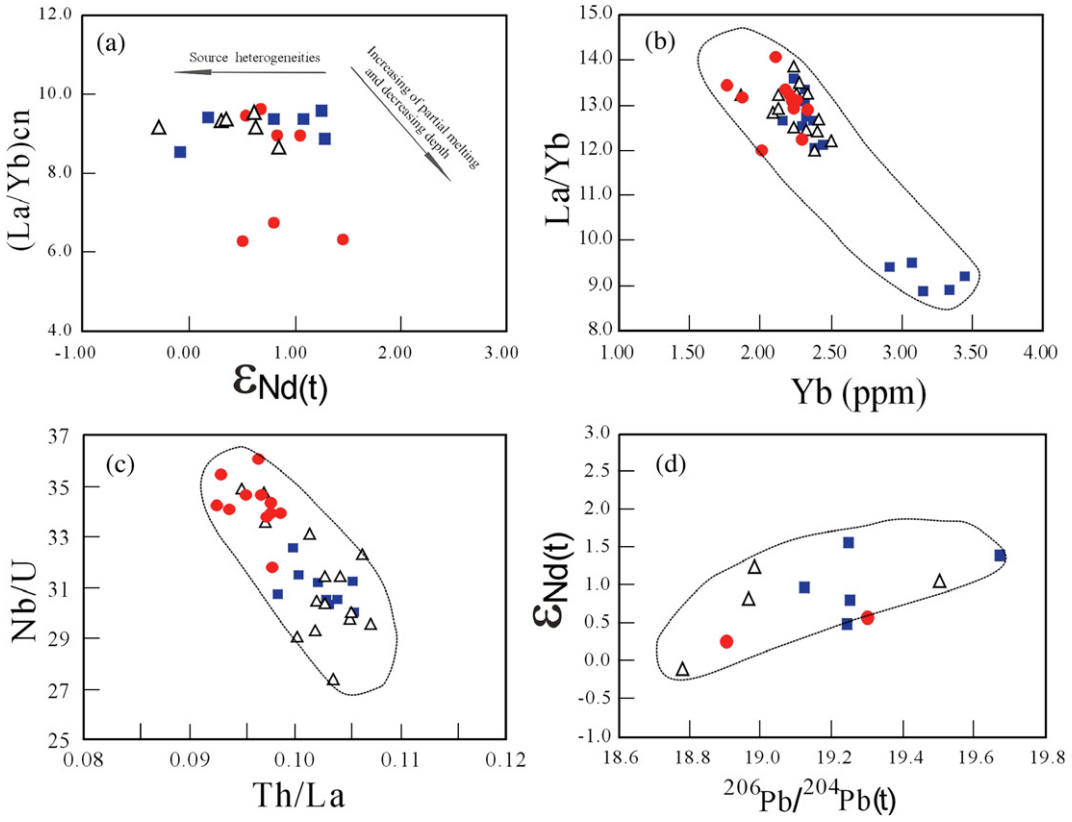

Fig. 10. Plots of (a) $\varepsilon_{Nd}(t)$ vs (La/Yb)cn, (b) Yb vs La/Yb, (c) Th/La vs Nb/U and (d) $^{206}Pb/^{204}Pb$ vs $\varepsilon_{Nd}(t)$ for the Permian basalts in western Guangxi Province.

lithospheric component in the magma source, assuming that crustal assimilation en route was insignificant.

There are two kinds of subcontinental mantle (EM) sources: EM1 (related to carbonatitic metasomatism) and EM2 (attributed to subduction-related metasomatism). An EM1-type source is generally characterized by negative Zr–Hf anomalies and lower (Hf/Sm)n ratios relative to (Ta/La)n ratios, whereas an EM2-type source is characterized by negative Nb–Ta anomalies and lower (Ta/La)n ratios than (Hf/Sm)n ratios (Hart, 1984, 1988; Palacz and Saunders, 1986; Weaver, 1991; Carlson, 1995; LaFlèche et al., 1998). The western Guangxi samples have (Hf/Sm)n ratios of 0.79–1.10 and (Ta/La)n ratios of 0.76–0.97, suggesting the involvement of a carbonatitic metasomatised component. On the plots of Sr–Pb and Pb–Pb isotopes (Fig. 7a–c), they have $(^{87}Sr/^{86}Sr)_i$, $(^{207}Pb/^{204}Pb)i$ and $(^{208}Pb/^{204}Pb)i$ ratios lower than an EM2-type source with comparable $(^{206}Pb/^{204}Pb)i$ ratios, and appear to be more compatible with an EM1-type source. Thus, we argue that the elemental ratios and Sr, Nd and Pb isotopic compositions for these samples define a binary mixing array between EM1 and HIMU components, supporting our suggestion that they are the products of the plume-lithosphere interaction.

5.2. Petrogenetic model related to the Emeishan LIP

Recent SHRIMP zircon U–Pb data for the mafic–ultramafic intrusions spatially associated with the Emeishan LIP show that these intrusive rocks have a crystallization age of ~260 Ma (Zhou et al., 2002a,b, 2006; Guo et al., 2004). For example, the Xinjie ultramafic (western Sichuan Province) and the Anding mafic intrusions (southeastern Yunnan Province) yielded weighted mean $^{206}Pb/^{238}U$ ages of 259±3 Ma and 258±3 Ma, respectively (Zhou et al., 2002a,b, 2006). The Yanyuan diabasic dike, the Panzhihua intrusion (western Sichuan), and the Shadou diabasic sill (eastern Yunnan) have geochemical affinities with the Emeishan high-Ti basalts, and have weighted mean $^{206}Pb/^{238}U$ ages of 262±3 Ma (Guo et al., 2004) and 260±3 Ma (Zhou et al., 2006), respectively. Previous geochronological data for the Emeishan flood basalts are dominantly $^{40}Ar/^{39}Ar$ plateau ages that are younger than

256 Ma (e.g., Boven et al., 2002; Lo et al., 2002; Ali et al., 2004; Fan et al., 2004). As mentioned above, the two representative basalt samples from western Guangxi Province have SHRIMP zircon U–Pb ages of ~259 Ma, representing the eruption time of these rocks. This age is identical to that for the mafic–ultramafic intrusions associated with the Emeishan LIP within the stated error (~260 Ma; Zhou et al., 2002a,b, 2006; Guo et al., 2004), indicating a synchronous magmatic event. Therefore, the primary magmatism of the Emeishan LIP occurred over a short time interval (~2–3 Ma) at ~260 Ma (end-Guadalupian), supporting the previous hypothesis proposed by Yin et al. (1992) and Jin and Shang (2000). Our new data presented above also favor the scenario that the Guangxi basalts are spatially and temporally associated with the Emeishan LIP.

The basalts in western Guangxi Provinces are geochemically comparable with Emeishan high-Ti basalts and the associated high-Ti intrusions in the Inner and Intermediate Zones (e.g., Xu et al., 2001; Xiao et al., 2003, 2004a,b; Zhou et al., 2006). The elemental and isotopic variability of the Guangxi basalts is likely due to low degrees of melting of a heterogeneous garnet-bearing mantle. Furthermore, the magma source reservoir may have contained both HIMU- and EM1-components. The HIMU-type source is most likely related to the Emeishan plume, whereas the EM1 component can be linked to the Yangtze continental lithosphere (e.g., Wang et al., 2003; Zhou et al., 2006). Thus, the EM1- and HIMU-type components suggest that the Emeishan plume impacted the basement of the Yangtze continental lithosphere, resulting in plume-lithosphere interaction and erosion of the subcontinental lithosphere. Laboratory and numerical results provide two possible explanations for low-degrees of melting of plume materials (e.g., Griffiths and Campbell, 1990). These are: (1) the plume is at a steady state; and (2) the plume is far from the plume axis. However, the influence of the HIMU component for the plume-derived magma is more significant during its initiation than when it reaches a steady state, and gradually decreases with the development of the plume. Taking into account other available data (Song et al., 2001; Xu et al., 2001, 2004; Zhang and Wang, 2002; Xiao et al., 2003; Zhou et al., 2006), we argue that the Guangxi basalts were most likely generated at the periphery of the plume. Thus, we further infer that the Emeishan high-Ti basalts were formed by a low degree of partial melting of a mixed source with both EM1- and HIMU-type components, distinct from that of the Emeishan low-Ti basalts.

He et al. (2003, 2006)) concluded that a kilometer-scale crustal doming with <3 Ma duration might have occurred prior to the rapid eruption of the voluminous Emeishan LIP, and proposed that the LIP can be spatially divided into Inner, Intermediate and Outer zones on the basis of the magnitude of uplift. However, few data support the occurrence of Emeishan basalts and associated rocks in the Outer zones. Our reappraisal of the basalts in western Guangxi provides important evidence indicating that the Emeishan LIP not only occurred in the Outer zone, but also extended over a broader region than previously thought. It is very possible that large portions of the Emeishan LIP exist in the Outer zone but are buried under widespread Mesozoic strata in SW China. This interpretation would greatly increase the original estimates for the volume of the Emeishan LIP (e.g., Gan, 1991; Song et al., 2001; He et al., 2003, 2006; Zhou et al., 2006).

Acknowledgements

We thank L. Qi for his help with the ICP-MS analyses and R.-H. Zhang for assistance with the Sr–Nd isotope analyses. Drs. Y.-G. Xu and Y.-H. Zhang provided many thoughtful discussions and suggestions. Critical and constructive reviews by P. T. Robinson, P. C. Lightfoot, L. Xiao and M.-F. Zhou were a great help in improving the manuscript. This study was financially supported by from the China Natural Science Foundation (projects 40421303 and 40334039), the Chinese Academy of Sciences (project kzcx2-yw-128) and China Petroleum & Chemical Corporation Grants.

References

Ali, J.R., Lo, C.H., Thompson, G.M., Song, X.Y., 2004. Emeishan basalt Ar–Ar overprint ages define several tectonic events that affected the western Yangtze platform in the Mesozoic and Cenozoic,. J. Asian Earth Sci. 23, 163–178.

Arndt, N.T., Chauvel, C., Fedorenko, V., Czamanske, G., 1998. Two mantle sources, two plumbing systems: tholeiitic and alkaline magmatism of the Maymecha River basin, Siberian flood volcanic province. Contrib. Mineral. Petrol. 133, 297–313.

Arndt, N.T., Czamanske, G.K., Walker, R.J., Chauvel, C., Fedorenko, V.A., 2003. Geochemistry and origin of the intrusive hosts of the Noril'sk–Talnakh Cu–Ni–PGE sulfide deposits. Econ. Geol. 98, 495–515.

Barling, J., Goldstein, S.L., 1990. Extreme isotopic variations in Heard Island lavas and the nature of mantle reservoirs. Nature 348, 59–62.

Boven, A., Pasteels, P., Punsalan, L.E., Liu, J., Luo, X., Zhang, W., Guo, Z., Hertogen, J., 2002. $^{40}Ar/^{39}Ar$ geochronological constraints on the age and evolution of the Permo-Triassic Emeishan volcanic province, southwest China. J. Asian Earth Sci. 20, 157–175.

Carlson, R.W., 1995. Isotopic inferences on the chemical structure of the mantle. J. Geodyn. 20, 365–386.

Chung, S.L., Jahn, B.M., 1995. Plume-lithosphere interaction in generation of the Emeishan flood basalts at the Permian–Triassic boundary. Geology 23, 79–93.

Compston, W., Williams, I.S., Meyer, C., 1984. U–Pb geochronology of zircons from Lunar Breccia 73217 using a sensitive high mass resolution ion microprobe. J. Geophys. Res. 89, 525–534.

Deniel, C., 1998. Geochemical and isotopic (Sr, Nd, Pb) evidence for plume-lithosphere interactions in the genesis of Grande Comore magmas (Indian Ocean). Chem. Geol. 144, 281–303.

DePaolo, D.J., 1981. Trace element and isotopic effects of combined wall rock assimilation and fractional crystallization. Earth Planet. Sci. Lett. 53, 189–202.

Duprè, B., Allègre, C.J., 1983. Pb–Sr isotopic variation in Indian Ocean basalts and mixing phenomena. Nature 303, 142–146.

Fan, W.M., Wang, Y.J., Peng, T.P., Miao, L.C., Guo, F., 2004. Ar–Ar and U–Pb geochronology of Late Paleozoic basalts in western Guangxi and its constraints on the eruption age of Emeishan basalt magmatism. Chin. Sci. Bull. 49 (21), 318–2327.

Frey, F.A., Garcia, M.O., Roden, M.F., 1994. Geochemical characteristics of Koolau Volcano: implications of intershield geochemical differences among Hawaiian volcanoes. Geochim. Cosmochim. Acta 58, 1441–1462.

Gan, J.Y., 1991. Spatial and temporal distribution of Emeishan basaltic rocks in three southwestern province (Sichuang, Yunnan and Guizhou) of China. Chin. Sci. Bull. 12, 923–932.

Griffiths, R.W., Campbell, I.H., 1990. Stirring and structure in mantle starting plume. Earth Planet. Sci. Lett. 99, 66–78.

Guo, F., Fan, W.M., Wang, Y.J., Li, C.W., 2004. When did the Emeishan mantle plume activity start? Geochronological and geochemical evidence from ultramafic–mafic dykes in southwestern China, Intern. Geol. Rev. 46, 226–234.

GXBGMR (Guangxi Bureau Geological Mineral Resource), 1985. Regional geology of Guangxi. Geol. Pub. House, Beijing, pp. 1–853.

GZBGMR (Guizhou Bureau Geological Mineral Resource), 1987. Regional geology of Guizhou Province. Geol. Pub. House, Beijing, pp. 1–698.

Hamelin, B., Allègre, C.J., 1985. Large scale regional units in the depleted upper mantle revealed by an isotopic study of the south–west India ridge. Nature 315, 196–198.

Hart, S.R., 1984. The Dupal anomaly: a large-scale isotopic anomaly in the southern hemisphere. Nature 309, 753–756.

Hart, S.R., 1988. Heterogeneous mantle domains: signature, genesis and mixing chronologies. Earth Planet. Sci. Lett. 90, 273–296.

Hart, S.R., Gerlach, D.C., White, W.M., 1986. A possible new Sr–Nd–Pb mantle array and consequences for mantle mixing. Geochim. Cosmochim. Acta 50, 1551–1557.

Hawkesworth, C.J., Rogers, N.W., van Calsteren, P.W.C., Menzies, M.A., 1984. Mantle enrichment processes. Nature 311 (27), 331–335.

He, B., Xu, Y.G., Chung, S.L., Wang, Y.M., Luo, Z.Y., 2006. Sedimentation and lithofacies paleogeography in southwestern China before and after the Emeishan flood volcanism: New insights into surface response to mantle plume activity. J. Geol. 114, 117–132.

He, B., Xu, Y.G., Chung, S.L., Xiao, L., Wang, Y.M., 2003. Sedimentary evidence for a rapid, kilometer-scale crustal doming prior to the eruption of the Emeishan flood basalts, Earth Planet. Sci. Lett. 213, 391–405.

Hofmann, A.W., Jochum, K.P., Seufert, M., White, W.M., 1986. Nb and Pb in oceanic basalts: new constraints on mantle evolution. Earth Planet. Sci. Lett. 79, 33–45.

Hollanda, M.H.B.M., Pimentel, M.M., Oliveira, D.C., Jardim de Sá, E.F., 2006. Lithosphere–asthenosphere interaction and the origin of Cretaceous tholeiitic magmatism in Northeastern Brazil: Sr–Nd–Pb isotopic evidence. Lithos 86, 34–49.

Jin, Y., Shang, J., 2000. The Permian of China and its interregional correlation. In: Yin, H., Dickins, J.M., Shi, G.R., Tong, J. (Eds.), Permian–Triassic evolution of Tethys and western Circum–Pacific: Developments in Palaeontology and Stratigraphy, vol. 18. Elsevier Press, Amsterdam, pp. 71–98.

LaFlèche, M.R., Camiré, G., Jenner, G.A., 1998. Geochemistry of post-Acadian, Carboniferous continental intraplate basalts from the Maritimes basin, Magdalen islands, Québec, Canada. Chem. Geol. 148, 115–136.

Lassiter, J.C., DePaolo, D.J., 1997. Plume/lithosphere interaction in the generation of continental and oceanic flood basalts: chemical and isotopic constraints. In: Mahoney, J.J., Coffin, M.F. (Eds.), Large Igneous Province: Continental, Oceanic, and Planetary Flood Volcanism, American Geophysical Union Geophysical Monograph, vol. 100, pp. 335–355.

LeBas, M.J., LeMaitre, R.W., Streckeisen, A., Zanettin, B., 1986. A chemical classification of volcanic rocks based on the total alkali-SiO_2 diagram. J. Petrol. 27, 745–750.

Lightfoot, P.C., Hawkesworth, C.J., Hergt, J., Naldrett, A.J., Gorbachev, N.S., Fedorenko, V.A., Doherty, W., 1994. Chemostratigraphy of Siberian trap lavas, Noril'sk district, Russia: implications for the evolution of flood basalt magmas. In: Lightfoot, P.C., Naldrett, A.J. (Eds.), Proceedings of the Sudbury–Noril'sk Symposium. Ont. Geol. Surv. Spec., vol. 5, pp. 283–312.

Lo, C.H., Chung, S.L., Lee, T.Y., Wu, G.Y., 2002. Age of the Emeishan flood magmatism and relations to Permian–Triassic boundary events. Earth Planet. Sci. Lett. 198, 449–458.

Ludwig, K.R., 2001. Sqiud 1.02: A user manual. Berkeley Geochronological Center Special Publication, pp. 1–219.

Ma, Y.X., Ji, X.T., Li, J.C., Huang, M., Min, Z.Z., 2003. Mineral resources of Panzhihua, Sichuan Province, SW China. Chengdu Univ. Techno. Press, Chengdu, p. 275.

Palacz, Z.A., Saunders, A.D., 1986. Coupled trace element and isotope enrichment in the Cook–Austral– Samoa islands, southwest Pacific. Earth Planet. Sci. Lett. 79, 270–280.

Qi, L., Hu, J., Gregoire, D.C., 2000. Determination of trace elements in granites by inductively coupled plasma-mass spectrometry. Talanta 51, 507–513.

Qiu, Y.M., Gao, S., McNaughton, N.J., Groves, D.I., Ling, W.L., 2000. First evidence of >3.2 Ga continental crust in the Yangtze craton of South China and its implications for Archaean crustal evolution and Phanerozoic tectonics. Geology 28 (1), 11–14.

Roden, M.F., Trull, T., Hart, S.R., Frey, F.A., 1994. New He, Nd, Pb and Sr isotopic constraints on the constitution of the Hawaiian plume: results from Koolau Volcano Oahu, Hawaii, USA. Geochim. Cosmochim. Acta 58, 1431–1440.

Song, B., Zhang, Y.H., Wang, Y.S., 2002. Mount making and procedure of the SHRIMP dating. Geol. Rev. 48, 26–30.

Song, X.Y., Zhou, M.F., Hou, Z.Q., Cao, Z., Wang, Y., Li, Y., 2001. Geochemical constraints on the mantle source of the Upper Permian Emeishan continental flood basalts, southwestern China. Internatl. Geol. Rev. 43, 213–225.

Sun, S.S., McDonough, W.F., 1989. Chemical and isotopic systematics of oceanic basalts: implications for mantle composition and processes. In: Saunders, A.D., Norry, M.J. (Eds.), Magmatism in the ocean basins, 42. Geol. Soc. Spec. Pub., pp. 313–345.

Taylor, S.R., McLennan, S.M., 1985. The continental crust: Its composition and evolution. Oxford Press Blackwell, pp. 1–312.

Wang, Y.J., Fan, W.M., Guo, F., Peng, T.P., Li, C.W., 2003. Geochemistry of Mesozoic mafic rocks around the Chenzhou–Linwu fault, South China: Implications for the lithospheric boundary between Yangtze and Cathaysia blocks. Internatl. Geol. Rev. 45 (4), 263–286.

Wang, Z.C., Wu, H.R., Kuang, G.D., 1997. Characteristics of the late Paleozoic oceanic basalts and their eruptive environment in Western Guangxi. Acta Petrol. Sinica 13, 260–265.

Weaver, B.L., 1991. The origin of ocean island basalt end-member compositions: trace element and isotopic constraints. Earth Planet. Sci. Lett. 104, 381–397.

Williams, I.S., Claesson, S., 1987. Isotope evidence for the Precambrian province and Caledonian metamorphism of high grade paragneiss from the Seve Nappes, Scandinavian Caledonides, II. Ion microprobe zircon U–Th–Pb. Contrib. Mineral. Petrol. 97, 205–217.

Winchester, J.A., Floyd, P.A., 1977. Geochemical discrimination of different magma series and their differentiation products using immobile elements. Chem. Geol. 20, 325–343.

Wu, H.Y., Kuang, G.D., Wang, Z.C., 1993. Reinterpretation of basic igneous rocks in western Guangxi and its tectonic implications. Scientia Geol. Sinica 28, 288–289.

Xiao, L., Xu, Y., Chung, S.L., He, B., Mei, H., 2003. Chemostratigraphic correlation of Upper Permian lavas from Yunnan Province, China: extent of the Emeishan large igneous province. Internatl. Geol. Rev. 45, 753–766.

Xiao, L., Xu, Y.G., Mei, H.J., Zheng, Y.F., He, B., Pirajno, F., 2004a. Distinct mantle sources of low-Ti and high-Ti basalts from the western Emeishan large igneous province, SW China: implications for plume-lithosphere interaction. Earth Planet. Sci. Lett. 228, 525–546.

Xiao, L., Xu, Y.G., Xu, J.F., He, B., Pirajno, F., 2004b. Chemostratigraphy of flood basalts in the Ganze–Litang region and Zhongza Block: implication for a western extension of the Emeishan large igneous province, SW China. Acta Geol. Sin., J. Geol. Soc. China 78, 61–67.

Xu, Y.G., Chung, S.L., Jahn, B.M., Wu, G.Y., 2001. Petrologic and geochemical constraints on the petrogenesis of Permian–Triassic Emeishan flood basalts in southwestern China. Lithos 58, 145–168.

Xu, Y.G., He, B., Chung, S.L., Menzies, M.A., Frey, F.A., 2004. Geologic, geochemical, and geophysical consequences of plume involvement in the Emeishan flood-basalt province. Geology 32, 917–920.

Yin, H., Huang, S., Zhang, K., Hansen, H.J., Yang, F., Ding, M., Bie, X., 1992. The effects of volcanism of the Permo-Triassic mass extinction in South China. In: Sweet, W.C., Yang, Z.Y., Dickins, J.M., Yin, H.F. (Eds.), Permo-Triassic Events in the Eastern Tethys: Stratigraphy, Classification, and Relations with the Western Tethys. World and Regional Geology, vol. 2. Cambridge Univ. Press, Cambridge, pp. 146–157.

YNBGMR(Yunnan Bureau Geological Mineral Resource), 1990. Regional geology of Yunnan Province. Geol. Pub. House, Beijing, pp. 1–728.

Zhang, Q., Qian, Q., Wang, Y., 1999. Late Paleozoic basic magmatism from NW Yangtze margin and the evolution of the Paleo-Tethyan ocean. Acta Petrol. Sinica 15 (4), 576–583.

Zhang, Z.C., Wang, F.S., 2002. Geochemistry of two types of basalts of the Emeishan basaltic Province: evidence for mantle plume-lithosphere interaction. Acta Geol. Sinica 76 (2), 138–147.

Zhou, M.F., Malpas, J., Song, X., Kennedy, A.K., Robinson, P.T., Sun, M., Lesher, C.M., Keays, R.R., 2002a. A temporal link between the Emeishan large igneous province (SW China) and the end-Guadalupian mass extinction. Earth Planet. Sci. Lett. 196, 113–122.

Zhou, M.F., Yan, D.P., Kennedy, A.K., Li, Y.Q., Ding, J., 2002b. SHRIMP zircon geochronological and geochemical evidence for Neoproterozoic arc-related magmatism along the western margin of the Yangtze Block, South China. Earth Planet. Sci. Lett. 196, 51–67.

Zhou, M.F., Zhao, J.H., Qi, L., Su, W.C., Hu, R.Z., 2006. Zircon U–Pb geochronology and elemental and Sr–Nd isotope geochemistry of Permian mafic rocks in the Funing area, SW China. Contrib. Mineral. Petrol. 151, 1–19. doi:10.1007/s00410-005-0030-y.